1-1-1985

Laser-influenced fluorescence spectroscopy of rubidium atoms and mercury molecules.

Jan Szczesny Supronowicz
University of Windsor

Recommended Citation

Supronowicz, Jan Szczesny, "Laser-influenced fluorescence spectroscopy of rubidium atoms and mercury molecules." (1985). *Electronic Theses and Dissertations*. 6130.
https://scholar.uwindsor.ca/etd/6130

LASER-INDUCED FLUORESCENCE SPECTROSCOPY
OF Rb ATOMS AND Hg_2 MOLECULES

by

Jan Szczęsny Supronowicz

A Dissertation
submitted to the Faculty of Graduate Studies
through the Department of Physics
in Partial Fulfillment of the requirements
for the Degree of Doctor of Philosophy at
The University of Windsor

Windsor, Ontario, Canada

1985

ABSTRACT

Cross sections for 6^2D, 7^2D and 8^2D fine-structure mixing in Rb, induced in collisions with various ground-state atoms and N_2 molecules, have been determined using methods of atomic fluorescence. Rb vapour, pure or mixed with a buffer gas, was irradiated in a glass fluorescence cell with pulses of radiation from a N_2 laser-pumped dye laser, populating a ^2D fine-structure state by two-photon absorption. The resulting fluorescence included a direct component emitted in the decay of the optically excited state and a sensitized component due to the collisionally populated fine-structure state. Measurements of relative intensities of the two components in relation to buffer gas (or Rb vapour) pressure yielded the following cross sections.

Inelastic process	Cross sections (10^{-14} cm^2)						
	Rb	He	Ne	Ar	Kr	Xe	N_2
$6D_{3/2} \rightarrow 6D_{5/2}$	17.3	6.6	6.1	5.3	8.5	**	6.4
$6D_{3/2} \leftarrow 6D_{5/2}$	11.6	4.5	4.1	3.6	5.5	**	4.1
$7D_{3/2} \rightarrow 7D_{5/2}$	30	8.8	6.5	10.4	14.1	15.5	10.0
$7D_{3/2} \leftarrow 7D_{5/2}$	18	5.8	4.0	6.9	9.0	10.5	6.9
$8D_{3/2} \rightarrow 8D_{5/2}$	43.1	8.9	4.9	12.4	24.9	25.8	12.1
$8D_{3/2} \leftarrow 8D_{5/2}$	28.5	5.8	3.2	9.4	15.1	17.6	8.3

Cross sections for the effective depopulation of the ^2D doublets were also estimated.

The relative ordering among the cross sections for noble gases, which exhibit a minimum in the vicinity of neon or argon, has been found to be in good correlation with the variation of the elastic electron – noble gas scattering cross section. The cross sections for N_2 are virtually identical with those for Ar indicating that the molecular degrees of freedom play no important part in the interactions. The Rb–Rb cross sections exceed the other cross sections by a factor of 2–5, an effect ascribed to stronger interactions due to much larger polarizability of the ground-state Rb atoms.

The $G0_u^+$ state in Hg_2 'excimer' molecules (correlated with the 6^1P_1 atomic state) was populated by stepwise excitation through the metastable $A0_g^+$ state, and the fluorescence emitted in the $0_u^+ \longrightarrow X0_g^+$ decay was recorded with a spectrometer and a transient digitizer. The time evolution of the fluorescence indicated a very short (~1 ns) lifetime of the 0_u^+ excimer. The band corresponding to the v"=0 $(A0_g^+) \longrightarrow$ v'=0 $(G0_u^+)$ transition was identified in absorption and the energy separation of the two potential wells was determined as was the wavelength of the UV fluorescence emitted in the decay of the v'=0 level of the $G0_u^+$ state to the repulsive $X0_g^+$ ground state. An estimate was made of the vibrational frequency ω_e' and the anharmonicity $\omega_e' x_e'$ of the 0_u^+ state.

ACKNOWLEDGMENTS

I would like to express sincere thanks to Professor L. Krause for his support and constant attention which I enjoyed during my work as a graduate student at the Department of Physics, and for his patient and critical reading of the draft of this dissertation. I also wish to express my appreciation to Professor J.B. Atkinson and Professor M. Czajkowski for many enlightening discussions on the subject, and to Professors W.E. Baylis and G.W.F. Drake for their help in the theoretical interpretation of the results.

I owe special thanks to Dr. R.J. Niefer for his invaluable help in arranging the experimental apparatus, assistance in the measurements, and for writing the computer program controlling the experimental procedure in the second part of this work. Acknowledgments are due to Mr. W. Eberhart and Mr. A. Ditchburn for skillful preparation of the glassware, and to Mr. W. Grewe and the machine shop staff for constructing numerous elements of the apparatus. I am also indebted to Mr. B. Masse for servicing the electronic equipment used in the experiments, and to Mr. A. Buzzeo for the skillful and careful drafting of the figures.

To my fellow graduate students and to the staff of the Physics Department, I express thanks for creating an

excellent atmosphere of encouragement, especially important to me in the new environment.

Finally, I am grateful to the University of Windsor for financial assistance throughout the years of my graduate studies.

TABLE OF CONTENTS

LIST OF TABLES

LIST OF FIGURES

Page

I. INTRODUCTION

Experimental and theoretical studies of collisions between atoms and molecules continue to absorb the interest of a large variety of scientists and engineers. Of particular interest are inelastic collisions which generally cause changes in the internal state of the colliding partners or sometimes even in the very nature of the particles subjected to the collision. An analysis of collisional processes can yield information concerning the structure and configuration of the participating atoms, molecules or ions, and can also be useful in various applications involving laser (and other) plasmas, planetary and stellar atmospheres and chemical reactions. The knowledge of parameters governing collisional processes is particularly helpful in studies of non-equilibrium phenomena where it facilitates the formulation of theoretical models; these, in turn, can be used to predict experimental observations.

This dissertation gives an account of two separate experimental studies involving collisional processes. The first of these, presented in Chapter II, deals with inelastic transfer of excitation between $^2D_{3/2}$ and $^2D_{5/2}$ fine-structure states of rubidium atoms excited to intermediate energy levels. In the course of the second study (presented in Chapter III) an Hg_2 excimer is formed by a process involving inelastic collisions and is probed by emission and absorption spectroscopy.

Collisional excitation transfer between highly excited alkali atoms has been, for some time, the subject of numerous theoretical and experimental investigations. Fine-structure mixing in atoms excited to ^2P resonance states, being perhaps the easiest to realize using excitation with ordinary resonance lamps, was studied in this and many other laboratories (Krause 1975). The excitation process is less straightforward for higher atomic states because of selection rules and much smaller oscillator strengths, and it is necessary to use laser radiation to put the atoms into the desired excited states. This may be done by various methods, such as stepwise excitation, two-photon absorption, or electric quadrupole transition. In recent years there have been several reports of experiments involving n^2D states in various alkali-metal atoms. Experimental studies with sodium were carried out by Biraben et al. (1979) and Gallagher et al. (1977); experiments on rubidium were performed by Hugon et al. (1980a,b), by Schuessler's group (Hill et al. 1982; Zollars et al. 1983; Parker et al. 1984), and in this laboratory (Głódź et al. 1981; Wolnikowski et al. 1982; Supronowicz et al. 1984, 1985). Similar investigations with caesium were reported by Tam et al. (1978), Deech et al. (1977), and Rosiński and Sirko (1984).

The ^2D fine-structure mixing and quenching processes have also been the subject of several theoretical studies. Pascale (1978) calculated the cross sections for the $4^2D_{5/2} \rightarrow 4^2D_{3/2}$ fine-structure transition in sodium induced by collisions with ground-state noble-gas atoms. Prunelé and Pascale (1979) carried out theoretical calculations for the quenching of n^2D and n^2F alkali Rydberg states. More general cases of atoms in Rydberg states colliding with neutral particles were considered by Omont (1977) and Hahn (1981). Most of the above theoretical treatments assume the "free electron" model of the collision, which is not a particularly good model for the case of "intermediate" excited states that lie above the resonance levels, but not so high as to be regarded as "true" Rydberg states. A more complete analysis of collisions involving excited alkali atoms and ground-state noble gas atoms should include three-body molecular effects, including the valence electron of the excited atom, the remaining ionic core and the perturbing particle (Masnou-Seeuws et al. 1982 and references therein). Thus far no such calculations have been reported in the literature.

Chapter II presents the results of an experimental investigation of fine-structure mixing in 6^2D, 7^2D, and 8^2D Rb atoms, induced in collisions with ground-state Rb atoms, noble gas atoms and N_2 molecules. Rb atoms, excited by two-photon absorption to one of the fine-structure sublevels, decay radiatively to a lower state or are collisionally transferred to the other fine-structure sublevel. There is also the possibility of collisional quenching (depopulation) of the excited state, a process in which the ^2D states decay non-radiatively and their excitation energy is transferred to the manifold of lower-lying states. The spontaneous decay of ^2D Rb atoms to the $5^2P_{3/2}$ or $5^2P_{5/2}$ state causes the emission of fluorescent light. The observed fluorescence spectrum normally consists of two components: the direct component originating from the optically excited state and the sensitized fluorescence component which arises from the collisionally populated state. Since sensitized fluorescence appears as the result of transfer between the ^2D states induced in collisions with ground-state atoms and molecules, a variation in their density causes a corresponding change in the ratio of sensitized-to-direct fluorescent intensity, from which it is possible to extract the inelastic collision cross sections, if all the other physical parameters in the experiment are known or measurable.

The experimental study of the Hg_2 excimer, presented in Chapter III, constitutes another example of a collision-related phenomenon, since the excited Hg_2 dimers are formed as the result of collisions involving mercury atoms and molecules in various quantum states. Quantitative information concerning the molecular states of Hg_2 has been obtained only recently from theoretical and experimental studies of the mercury excimers. The mercury atom, having two valence electrons, behaves like a spinless (J=0) particle in its ground 6^1S_0 state. Accordingly, the interaction between two such atoms is of a very weak van der Waals type, with an r^{-6} interaction potential giving rise to a shallow ground-state potential well whose depth with respect to the ground-state atomic level is estimated to be 450 cm^{-1}± 20% (Baylis 1977; Drullinger et al. 1977). Because a three-body collision is required to form a stable ground-state Hg_2 molecule while only a two-body collision suffices to dissociate it, and because of the Boltzmann distribution, the number of bound ground-state molecules constitutes a very small fraction of the ground-state Hg atoms.

When an interaction takes place between two Hg atoms, each in a different quantum state, the situation is somewhat different. There is degeneracy of energy levels at large r-values, corresponding to the exchange of excitation energy between the atoms and leading to the splitting into gerade and ungerade states at smaller r-values. The instantaneous interaction between the atoms leads to a first-order perturbation. If, for instance, one atom is in an S, and the other in a P state, the perturbation is proportional to r^{-3} when averaged over the electronic motion (Herzberg 1950). Consequently, the binding is stronger and the resulting Hg_2 molecule remains bound until its radiative or collisional decay and final dissociation. Such molecules, which have stable bound states only as excited species, are known as excited dimers or 'excimers'.

Figure I.1 shows the approximate potential energy curves for some Hg_2 states. The indicated binding energies and potential minima agree with the latest available spectroscopic and theoretical data (Niefer et al. 1983a). A considerable amount of theoretical work has been done by Hay et al. (1976), Mies et al. (1978), Baylis (1977) and Smith et al. (1977) aimed at calculating the shapes of the molecular potential curves and their relative energy separations.

The existence of the 3350 Å band, together with another band centered at 4850 Å, was first reported by Phillips (1913). Franck and Grotrian (1921) suggested, that electronically excited Hg_2 molecules were the origin of the two bands. Mrozowski (1937, 1944) put forward the hypothesis, that an 0_u^- molecular state correlated with the Hg 6^3P_0 atomic state was the carrier of the green 4850 Å emission band while a 1_u state correlated with the Hg 6^3P_1 state was responsible for the 3350 Å band. More recent experiments (Drullinger et al. 1977) and theoretical considerations presented by the same group (Smith et al. 1977) led to the conclusion that Mrozowski's assignments were only partly correct and that, while the 3350 Å band was indeed due to the radiative decay of the $D1_u$ state, the 4850 Å emission resulted from the radiative decay of a strongly bound Hg_3 trimer. These investigations also provided the best current estimates for the energy of the

Figure I.1. Potential energy diagram showing assignments of some Hg_2 states (Niefer et al. 1983a,b; Mies et al. 1978), positions of relevant Hg states, and the extent of the v'=57, $G0_u^+ \longrightarrow X0_g^+$ transitions (Ehrlich and Osgood 1978, 1979).

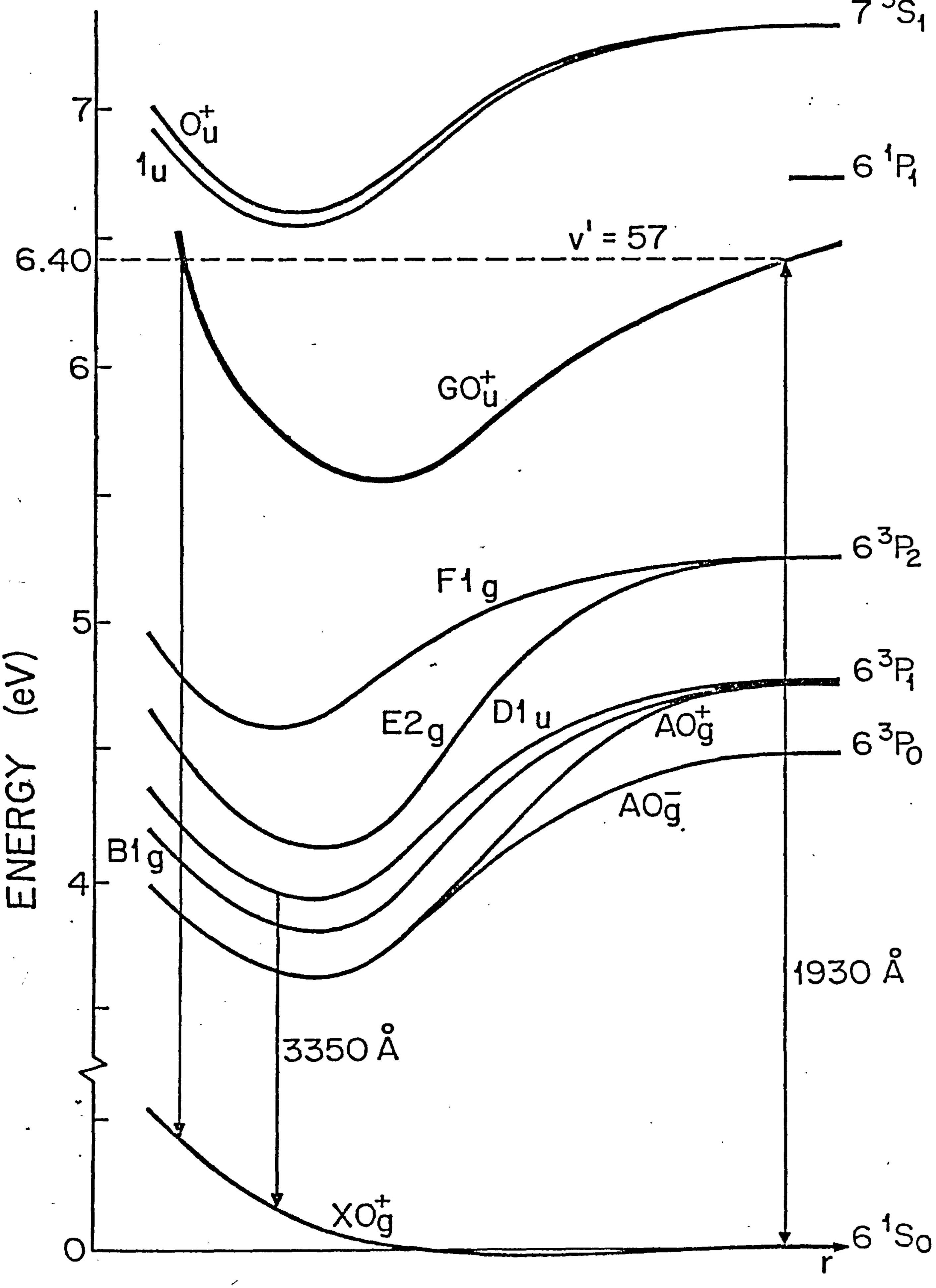
ENERGY (eV)
7
6.40
6
5
4
0
r
$7\,^3S_1$
$6\,^1P_1$
$6\,^3P_2$
$6\,^3P_1$
$6\,^3P_0$
$6\,^1S_0$
0_u^+
1_u
v' = 57
$G0_u^+$
$F1_g$
$E2_g$
$D1_u$
$A0_g^+$
$A0_g^-$
$B1_g$
$X0_g^+$
3350 Å
1930 Å

lowest-lying metastable $A0_g^{\pm}$ states of the Hg_2 excimer.

Takeyama (1952) observed, in the visible spectral region, a large number of fluorescent bands emitted from mercury vapour, but attempted virtually no assignments of the bands to particular transitions. Callear and Lai (1979, 1980, 1982) reported a series of flash photolysis experiments in which they investigated numerous absorption bands in the visible and ultraviolet region, and were able to achieve a partial correlation with the emission bands of Takeyama. They proposed tentative assignments of the bands, which, in addition to the Hg_2 excimers, involved participation from Hg_3 excited trimers and Hg_2^+ excimer ions. More recently, a series of experiments performed in this laboratory (Niefer et al. 1983a,b) yielded the radiative decay times of several Hg_2 bands and led to the assignments of the observed wavelengths. A partial vibrational analysis of the $A0_g^{\pm}$, $E2_g$ and $F1_g$ states was also carried out in the course of the investigation.

The present study, which constitutes an extension of the experiments of Niefer et al. (1983a,b), deals with the 2250 Å fluorescent band which has been known to exist for some time. This relatively strong and wide band, which extends from the Hg 1849.5 Å resonance line to approximately 2400 Å, was first reported by Hamada (1931), who used a hollow cathode discharge to excite mercury vapour in a fluorescence cell. Mrozowski (1930) observed structured side-bands on the short-wavelength side of the

2250 Å band, which he ascribed to 'bound-bound transitions' between vibrational levels of an upper Hg_2 state and the closely spaced levels of the shallow ground-state potential well. Drullinger et al. (1977) reported a 200 Å-wide fluorescent band centered at 2250 Å when probing the lower-lying metastable molecular states of mercury with 4880 Å argon-ion laser radiation, and suggested that the high-lying $G0_u^+$ state of Hg_2 was the carrier of this fluorescence.

Transitions involving the $G0_u^+$ state have also been studied by absorption spectroscopy. The $G0_u^+ \leftarrow X0_g^+$ transition was seen in absorption by Mrozowski (1930, 1934), and absorption of laser radiation, centered at 1930 Å, was used by Ehrlich and Osgood (1978, 1979) to 'photoassociate' the ground-state Hg atom pairs to high-lying vibrational levels of the $G0_u^+$ state. Ehrlich and Osgood used the term 'photoassociation' to describe the production of an Hg_2 excimer through absorption of a light quantum by a pair of ground-state Hg atoms which, at the moment of excitation, happen to be so close to each other that, immediately after the absorption, they are subjected to the strong binding potential associated with the excited state. The authors subsequently observed a Condon internal diffraction pattern in the fluorescence spectrum arising from the $G0_u^+ \longrightarrow X0_g^+$ transition.

In this investigation I have carried out a systematic study of collisional mixing between the fine-structure 6^2D,

7^2D and 8^2D states in rubidium using techniques of two-photon absorption and fluorescence spectroscopy of Rb vapour pure and mixed with a buffer gas in a fluorescence cell. I also attempted a more detailed study of the 2250 Å band structure using a 'pump and probe' technique to excite the GO_u^+ excimer state. The resulting fluorescence was recorded using methods of time-resolved spectroscopy and the analysis of the band profiles, resulting from excitation of particular GO_u^+ vibrational levels, yielded the vibrational constants and the energy at the minimum of the GO_u^+ potential curve.

II. FINE-STRUCTURE MIXING IN 6^2D, 7^2D AND 8^2D RUBIDIUM ATOMS BY COLLISIONS WITH GROUND-STATE ATOMS AND MOLECULES

1. Theory

a) Collisional processes

The cross section for an atomic process is visualized in semiclassical terms, as an imaginary area perpendicular to the trajectory of the striking particle, with which the trajectory of the incident particle intersects in order that the process should occur with a probability of 100%; if the area and trajectory do not intersect then no interaction takes place. This intuitive concept is equivalent to the formal (semiclassical) definition of the cross section:

$$\sigma = 2\pi\int_0^\infty \varrho(b)\,b\,db, \qquad \text{(II.1)}$$

where the probability ϱ of the process is some function of the impact parameter b ($\varrho \leq 1$). This definition, however, is valid only for a particular value of the relative velocity between the colliding partners and is not particularly useful for the interpretation of experiments in which the particles have a Maxwell-Boltzmann distribution of kinetic energy. This is because, even for the same partners, the collision cross sections may differ significantly at various velocities, depending on the mechanism governing the collisional process, that predominates within a particular range of velocities. The quantity which is actually measured in a vapour or gas enclosed in a cell, is the cross section Q(T) averaged over the Maxwell-Boltzmann velocity distribution corresponding to a particular temperature T:

$$Q(T)=\frac{\int_0^\infty \sigma(v)P(v,T)v\,dv}{\int_0^\infty P(v,T)v\,dv}\,, \qquad \text{(II.2)}$$

where $\sigma(v)$ is the velocity-dependent differential cross section. This formulation of the effective cross section is especially useful and relevant in experiments in which the efficiency of collisional excitation transfer between two atomic states is being investigated in gas or vapour cells. The present investigation is concerned with the phenomenon of change in the quantum state of an excited Rb atom, caused by collisions with various ground-state atoms and molecules. Since this change is mainly confined within the fine-structure doublet, the atom remains excited but is transferred to another quantum state with slightly different energy; the energy balance is interconverted with the kinetic energy of the colliding partners. The process is known as 'inelastic excitation transfer'. If the number of excited 'target' atoms, undergoing collisional transitions, is a very small fraction of the ground-state atoms, it is reasonable to assume that a particular excited atom will undergo collisions almost solely with ground-state atoms. Consequently, the frequency, per excited atom, of collisions which cause excitation transfer, is given by:

$$Z = N_0 \bar{v}_r Q(T), \qquad (II.3)$$

where Z is the rate of collisional mixing, N_0 is the particle density of the ground-state atoms and $\bar{v}_r$ is the average relative speed of the colliding partners.

If long-range interactions between colliding partners (such as the Coulomb potential which plays a role in collisions between charged particles) are excluded, the interaction potential is often localized in a region of the order of atomic (or molecular) dimensions. This is the case with the Fermi (1934) potential which approximately describes the interaction of ground-state noble gas atoms colliding with atoms in very high Rydberg states:

$$V(R) = 2\pi L \left|\Psi(\vec{R})\right|^2 \qquad (II.4)$$

Here L is the electron - noble-gas scattering length, and $\Psi(\vec{R})$ is the electronic wave function of the Rydberg atom where $\vec{R}$ corresponds to the relative position of the perturber atom with respect to the ionic core of the Rydberg atom (Eq. II.4 assumes dimensionless atomic units). In such a situation it is very useful to compare the measured cross section with the geometrical cross section of the Rydberg atom, which corresponds to the region, where the electronic wave function has significant non-zero values. Even though this concept is somewhat arbitrary, it yields some measure of the atomic (Rydberg) size. Bethe and Salpeter (1955) calculated the geometrical cross section as a function of the effective principal quantum number n^* and the azimuthal quantum number l:

$$\sigma_g = (1/2)\pi a_0^2 n^{*2}[5n^{*2}+1-3l(l+1)], \qquad \text{(II.5)}$$

where a_0 is the Bohr radius (0.529 Å). The much smaller size of the ground-state atom contributing to the total geometrical cross section can often be neglected because of the $(n^*)^4$-dependence of the geometrical cross section.

b) Excitation and decay processes

Collisional excitation transfer between the n^2D Rb states may be represented by the following equations:

$$Rb(n^2D_{3/2})+Rb(5^2S_{1/2}) \leftrightarrow Rb(n^2D_{5/2})+Rb(5^2S_{1/2})+\Delta E, \qquad \text{(II.6)}$$

$$Rb(n^2D_{3/2})+A \leftrightarrow Rb(n^2D_{5/2})+A+\Delta E, \qquad \text{(II.7)}$$

where n denotes the principal quantum number, A represents a ground-state noble gas atom or a N_2 molecule and ΔE is the appropriate fine-structure energy splitting as listed in Table II.1.

TABLE II.1. Fine-structure splitting of n^2D Rb states

state	Δ E (cm^{-1})	Δ E (GHz)
6^2D	2.26	67.8
7^2D	1.51	45.3
8^2D	1.01	30.3

Figure II.1 presents a partial energy level diagram for Rb, showing the states involved in the experiment and the transitions between them. The $n^2D_{3/2}$ or $n^2D_{5/2}$ state is selectively excited by two-photon absorption using a nitrogen laser-pumped dye laser. The fluorescence resulting from the decay of the n^2D states can be spectrally isolated with a monochromator so that only transitions between the n^2D and 5^2P states need be considered. The $nD_{5/2}$ state may decay radiatively only to the $5P_{3/2}$ state, while the $nD_{3/2}$ state may decay either to the $5P_{1/2}$ state or to the $5P_{3/2}$ state. The spectral separation between the 5P doublet amounts to 238 cm^{-1} and could be easily resolved. However, the fine-structure splitting of the n^2D states is too small to be resolved by the monochromator. Consequently, the observed fluorescence spectrum always consisted of two components. When the $n^2D_{3/2}$ state was optically excited, the component A was due to direct fluorescence and component B to a mixture of direct and sensitized fluorescence. When, on the other hand, $n^2D_{5/2}$ was the primarily populated state, the fluorescent component C was

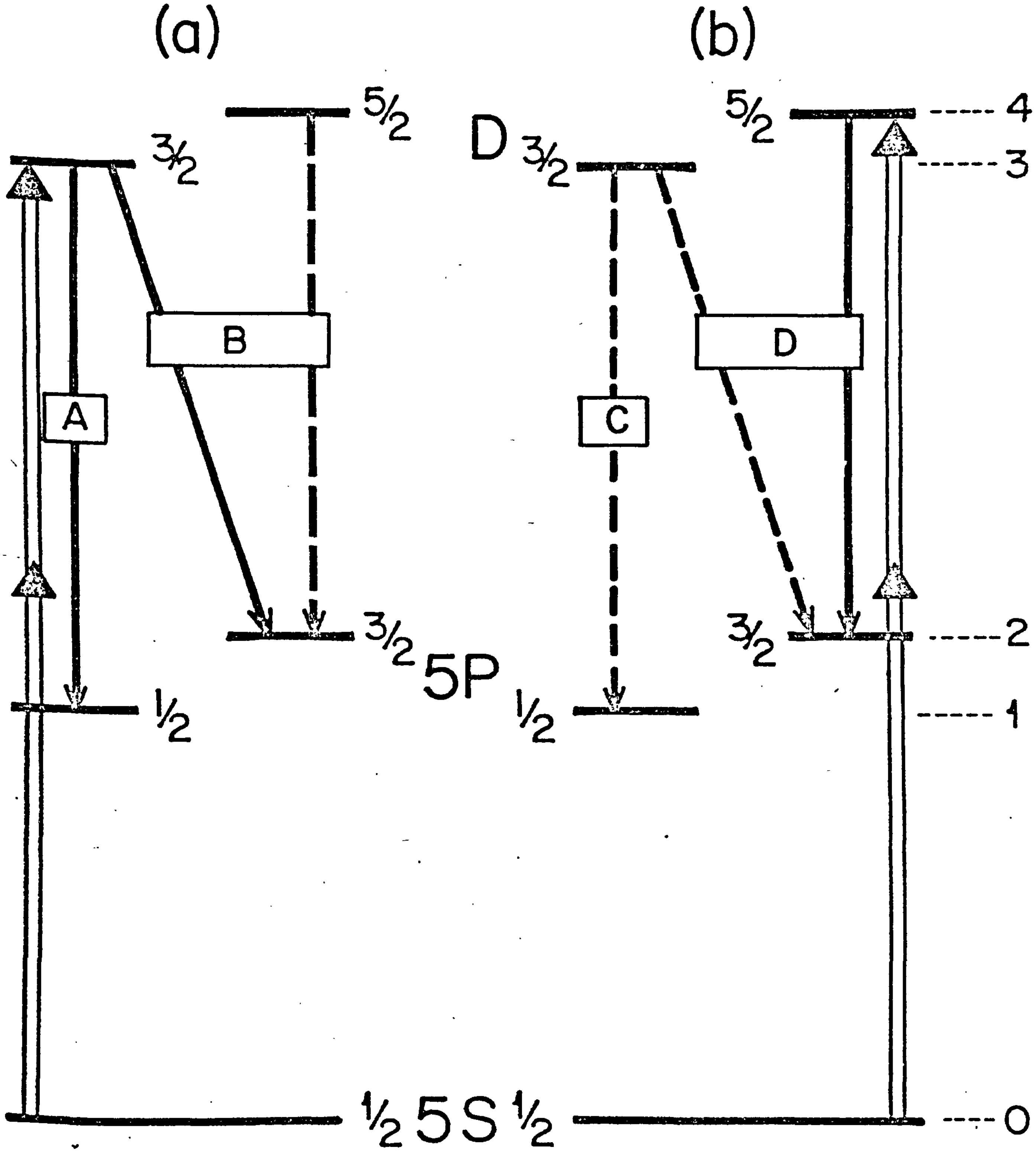
(a)
(b)
5/2
3/2
B
A
3/2
5P
1/2
D 3/2
5/2
D
C
3/2
1/2
4
3
2
1
0
1/2 5S 1/2

entirely due to sensitized fluorescence and component D to a mixture of direct and sensitized fluorescence. The wavelengths of all the involved transitions are listed in Table II.2.

TABLE II.2. Wavelengths of the radiative $n^2D \rightarrow 5^2P$ transitions (Å)

principal quantum number	TRANSITION		
n	$nD_{3/2}\rightarrow 5P_{1/2}$*	$nD_{3/2}\rightarrow 5P_{3/2}$+	$nD_{5/2}\rightarrow 5P_{3/2}$+
6	6206.3	6299.3	6298.4
7	5647.8	5724.6	5724.1
8	5362.6	5431.9	5431.6

*component A or C.

+component B or D.

The densities of the collisionally populated states may be represented by the appropriate rate equations. When the $n^2D_{3/2}$ state is optically excited (Fig. II.1a), the time-evolution of the population density of the $n^2D_{5/2}$ state is given by:

$$dN_4/dt = N_3N_0vQ_{34} - N_4(1/\tau_4+N_0vQ_{43}+N_0vQ_4); \qquad (II.8)$$

in the reverse case (Fig. II.1b):

$$dN_3/dt = N_4N_0vQ_{43} - N_3(1/\tau_3+N_0vQ_{34}+N_0vQ_3). \qquad \text{(II.9)}$$

In Eqs. (II.8) and (II.9) the symbols τ and N denote lifetimes and population densities of states indicated by the subscripts 1,2,3,4, corresponding to $5^2P_{1/2}$, $5^2P_{3/2}$, $n^2D_{3/2}$, and $n^2D_{5/2}$, respectively; N_0 is the density of the colliding partner (ground-state Rb atoms, noble-gas atoms or N_2 molecules); Q_{34} and Q_{43} are the total (thermally averaged) cross sections for transfers $^2D_{3/2}\rightarrow{}^2D_{5/2}$ and $^2D_{5/2}\rightarrow{}^2D_{3/2}$, respectively, and Q_3 and Q_4 are the effective quenching cross sections for collisional transfer to all other Rb states; $v=(8kT/\pi\mu)^{1/2}$ is the average relative speed of the colliding partners whose reduced mass is μ.

When pulsed excitation is employed, as is the case in this experiment, the populations of the ^2D states are time-dependent. Equations (II.8) and (II.9) can be solved and the ratio of time-averaged values $\bar{N}_3$ and $\bar{N}_4$ can be obtained from the solutions (Pace and Atkinson 1974):

$$\bar{N}_3/\bar{N}_4 = (1/\tau_4Q_{34})(1/N_0v)+(Q_{43}+Q_4)/Q_{34}; \qquad \text{(II.10)}$$

$$\bar{N}_4/\bar{N}_3 = (1/\tau_3Q_{43})(1/N_0v)+(Q_{34}+Q_3)/Q_{43}. \qquad \text{(II.11)}$$

In Eq. (II.10) $\bar{N}_4$ represents the time-averaged population produced by collisional excitation transfer and $\bar{N}_3$ is due to optical excitation; in Eq. (II.11) the reverse is the case. Since the measured time-integrated fluorescent intensity is proportional to the product of the appropriate population and Einstein A coefficient for the particular transition, the following relations are obtained for the fluorescent intensity ratios:

$$I(3\rightarrow1)/I(3\rightarrow2) = A_{31}/A_{32}, \qquad \text{(II.12)}$$

$$I(4\rightarrow2)/I(3\rightarrow2)=(\bar{N}_4/\bar{N}_3)\times(A_{42}/A_{32}). \qquad \text{(II.13)}$$

Equations (II.10-13) yield the following expressions for the dependence of the measured intensity ratios of the components A,B,C,D on the density of the collision partner. When the $n^2D_{3/2}$ state is optically excited:

$$\frac{1}{I_B/I_A-(A_{32}/A_{31})} = \frac{A_{31}}{A_{42}}\,\frac{1}{\tau_4 Q_{43}}\,\frac{1}{N_0 v} + \frac{A_{31}}{A_{42}}\,\frac{Q_{43}+Q_4}{Q_{34}}, \qquad \text{(II.14)}$$

when the $n^2D_{5/2}$ state is optically excited:

$$\frac{I_D}{I_C} = \frac{A_{42}}{A_{31}}\,\frac{1}{\tau_3 Q_{34}}\,\frac{1}{N_0 v} + \frac{A_{42}}{A_{31}}\,\frac{Q_{34}+Q_3}{Q_{43}} + \frac{A_{32}}{A_{31}}. \qquad \text{(II.15)}$$

The lifetimes τ_3 and τ_4 were assumed to be equal to each other and were calculated from transition probabilities quoted by Anderson and Zilitis (1964). The ratios of Einstein A coefficients which are listed in Table II.3, were calculated from oscillator strengths given by Migdałek and Baylis (1979), according to the formula (e.g. Woodgate 1970):

$$\frac{A_{ji}}{A_{lk}} = \frac{f_{ij}}{f_{kl}}\,\frac{(g_l/g_k)}{(g_j/g_i)}\left(\frac{\nu_{ij}}{\nu_{kl}}\right)^2, \qquad \text{(II.16)}$$

where f are oscillator strengths, g are the statistical weights of the states involved in the transition and ν are the transition frequencies.

TABLE II.3. Ratios of Einstein coefficients

Rb state	A_{31}/A_{42}	A_{32}/A_{31}
6^2D	0.7807	0.2154
7^2D	0.7985	0.2106
8^2D	0.8000	0.2100

2. Experimental

a) Description of the apparatus

A schematic arrangement of the apparatus is shown in Fig. II.2. The exciting radiation was emitted by a N_2 laser-pumped dye laser and, after attenuation by a neutral density filter (whenever necessary), was weakly focussed inside the fluorescence cell mounted in an oven and containing either pure Rb vapour or a mixture of Rb vapour with a buffer gas. The resulting fluorescence emitted at right-angles to the direction of excitation was analyzed with a monochromator and registered with a photon counter whose output was displayed by a printer.

The dye laser was set up in a Littman double-grating configuration (Littman 1978). It employed a magnetically stirred cell containing a dye solution. The dyes and the respective output wavelengths are listed in Table II.4.

Figure II.2. Schematic diagram of the apparatus. M is the monochromator, PM the photomultiplier tubes, PC the photon counter, P the printer, F-P the Fabry-Perot etalon, D the photodiode, F_N the neutral density filter, and F_C the color filter.

TABLE II.4. Laser dyes and output wavelengths used for excitation

state	dye	wavelength (Å)	molar concentration (in ethanol)
6^2D	Rh 610/Nile blue	6970	$3.8\times10^{-3}/8\times10^{-4}$
7^2D	Rh 6G/Cres. viol.	6603	$2.5\times10^{-3}/3.3\times10^{-3}$
8^2D	Rhodamine 640	6404	5×10^{-3}

The dye laser produced light pulses of 5 ns duration at a repetition rate of 25 Hz. The spectral width of the emitted light, which was monitored with a Fabry-Perot etalon, was about 5 GHz which is much less than the separations of the n^2D states. It was verified that the ^2D fine-structure substates were indeed excited selectively since, with the laser light tuned midway between the two sublevels, no fluorescence was observed.

The effective spectral width of the exciting radiation was doubled as the result of the two-photon absorption process and exceeded considerably the width of the single absorption line which, under the conditions typical for the experiment (low buffer-gas and Rb-vapour pressure), was essentially determined by Doppler broadening [$\Delta\nu=\nu(2kT\ln2/mc^2)^{1/2}$, where ν is the frequency of the transition] and therefore did not exceed 1 GHz.

The fluorescence cell, which was made of pyrex glass, was cylindrical in shape, 4 cm long and 2.5 cm in diameter. It had a sidearm 7 cm long and 1 cm in diameter, which was located below the cell's main body and contained liquid rubidium metal. The cell was connected to a vacuum and gas-filling system through a greaseless stopcock mounted inside the oven, which allowed the cell to be filled with variable gas pressures while preventing the loss of rubidium from the cell which was kept closed during the actual measurements. Such an arrangement has the advantage over sealed-off cells in that it permits the cell to be evacuated between experimental runs and cleansed of gaseous impurities which inevitably tend to desorb from the cell walls and frequently are more efficient in quenching the atomic fluorescence than the buffer gases. The oven was heated electrically and had a separately thermostated jacket surrounding the sidearm, through which silicone oil was circulated from an ultrathermostat. Several copper-constantan thermocouples were placed at various locations inside the oven. Their response was recorded with a Hewlett-Packard 7101B Strip Chart Recorder to provide monitoring of temperatures in the vicinity of the cell.

The monochromator used in the experiment was equipped with a flat 1200 l/mm diffraction grating. It had two exit slits which permitted the simultaneous detection of the two spectral components. The outgoing light signals were detected by two RCA C31034 cooled photomultipliers whose outputs were registered by the two channels of an Ortec 9315 photon counter preceded by two Ortec 9302 amplifier-discriminators.

In dealing with measured intensity ratios, Eqs. (II.14) and (II.15) assume that the spectral sensitivity of the intensity-measuring device is the same for both fluorescence components. From the spectral response curves provided by the manufacturer of the photomultipliers it was found that this assumption was justified to a very good approximation, since the difference in sensitivities never exceeded 2%.

The pressures of the gases in the vacuum system were at first measured with a liquid nitrogen-trapped McLeod gauge (Wolnikowski et al. 1982). However, it was found that for pressures of the order of 1 mtorr the gauge gave erroneous readings for Ne and Ar. This was probably caused by the streaming of mercury vapor to the cold trap, which impeded the diffusion of the gases to the gauge reservoir (Bennewitz and Dohmann 1965). In subsequent experiments (Supronowicz et al. 1984,1985) the McLeod gauge was replaced by a Convectron vacuum gauge which was calibrated against an MKS-Baratron 220B capacitance gauge. The direct use of the Baratron during actual measurements was found to be inconvenient since it tended to worsen the quality of the vacuum in the apparatus.

b) Experimental procedure

Natural rubidium of 99.9% nominal purity, supplied by Metron, Inc. of Allamuchy, N.J., was redistilled under vacuum and then distilled into the sidearm of the previously baked out cell. At the beginning of each experimental run, the system was baked and pumped down to 10^{-8} torr. The cell was then used for experiments with pure Rb vapour and with mixtures of Rb and several buffer gases. The saturated vapour pressure of rubidium was calculated from the lowest sidearm temperature using the following temperature-vapour pressure relation (Nesmeyanov 1963):

$$\log_{10}P = 15.88253 - 4529.635/T + \\ + 0.00058663\ T - 2.99138 \log_{10}T \qquad (II.17)$$

where P is the vapour pressure in torr. During the experiments with pure rubidium, the sidearm temperatures ranged from 373 K to 473 K, corresponding to a pressure range 0.18 - 38 mtorr. During each experimental run this temperature was maintained constant within ±0.2 K and was kept about 30 K below the cell temperature to prevent condensation on the windows. During the experiments with Rb-buffer gas mixtures the sidearm temperature was kept constant at 350 ± 0.2 K which corresponded to a Rb vapour pressure of 4×10^{-5} torr and provided a reasonable compromise between adequate fluorescent signals and sufficiently low Rb densities to render negligible the effects of Rb-Rb collisions. When measuring intensities of fluorescence components emitted from 7^2D and 8^2D states, the gas pressures were varied from about 1 mtorr to over 100 mtorr, above which the ratio of sensitized to direct fluorescence became insensitive to further changes in gas pressure. For the 6^2D states the efficiency of the excitation transfer collisions was found to be lower because of generally smaller values of the cross sections and shorter lifetimes, and it was necessary to employ buffer gas pressures up to 200 mtorr.

The photon counter was gated by the laser pulses, each of which activated the counter for a time span equivalent to about 10 lifetimes of the excited states so that virtually all the light emitted into the solid angle of observation could be recorded with a considerable reduction of background noise. The simultaneous registering of the intensities of both spectral components of the fluorescence also reduced errors arising from fluctuations in the laser intensity. The signal intensity was kept sufficiently low for the photon counter to distinguish between single pulses and avoid the "overlap" of two or more pulses. Since the counter was able to resolve two photons 10 ns apart and since an average of approx. 0.8 photons was detected during each active period of the counter, the probability of "photon overlap" was negligibly small, assuming a Poisson time-distribution of incoming photons. The possibility of scattered laser light being registered as an actual signal was excluded by placing a color cut-off edge filter in front of the monochromator entrance slit.

3. Results and Discussion

Equations (II.14) and (II.15) can be rewritten as follows:

$$\frac{A_{42}}{A_{31}}\left[\frac{I_B}{I_A}-\frac{A_{32}}{A_{31}}\right]^{-1}=\frac{1}{\tau}\,\frac{1}{Q_{34}}\,\frac{C\sqrt{T}}{P}+\frac{Q_{43}+Q_4}{Q_{34}}, \qquad \text{(II.18)}$$

$$\frac{A_{31}}{A_{42}}\left[\frac{I_D}{I_C}-\frac{A_{32}}{A_{31}}\right]=\frac{1}{\tau}\,\frac{1}{Q_{43}}\,\frac{C\sqrt{T}}{P}+\frac{Q_{34}+Q_3}{Q_{43}}. \qquad \text{(II.19)}$$

where $C=(\pi k\mu/8)^{1/2}$ and P is the pressure in the cell. When the experiment deals with the Rb*-Rb collisions, P represents the pressure of the Rb vapour. The plots of the left-hand sides of Eqs. (II.18) and (II.19) against $\sqrt{T}/P$ should be linear. This is indeed the case as may be seen in Figs. II.3-II.5 which show such plots for Rb*-Rb collisions in pure Rb vapour. Virtually all the experimental data points lie on straight lines which were generated by least-squares analyses. The slopes of the lines, when substituted in Eqs. (II.18) and (II.19), yield the cross sections Q_{43} and Q_{34} while the intercepts give the effective quenching cross sections Q_3 and Q_4. In the case of Rb*-Rb collisions, the error assigned to the values of Q_{43} and Q_{34} was 20%. The main sources of error appear to arise from the uncertainty in the Rb vapour pressure determined from the side-arm temperature, the sensitivity calibration of the two counter channels, and the ^{2}D lifetimes, with presumably smaller contributions arising

Figure II.3. A plot of the left-hand sides of Eqs. (II.18) and (II.19) against $\sqrt{T}/P$, illustrating Rb*-Rb collisional f.s. mixing of the 6^2D states. Rough values of Rb-vapour pressures are indicated along the abscissa. The error bars are representative of experimental error over the Rb-density range.

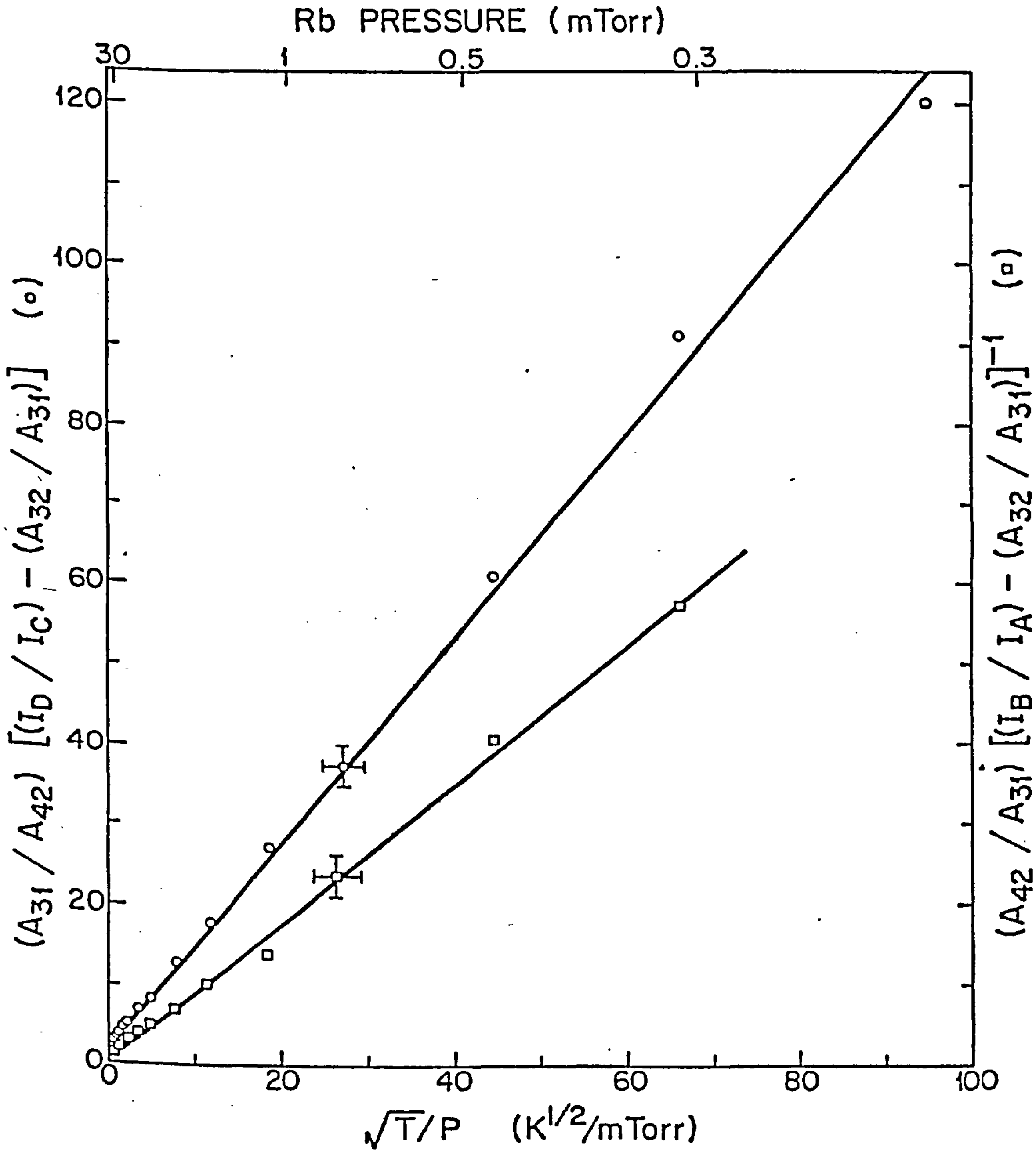
Rb PRESSURE (mTorr)
30
1
0.5
0.3
120
100
80
60
40
20
0
0
20
40
60
80
100
$(A_{31}/A_{42})\,[(I_D/I_C) - (A_{32}/A_{31})]$ (○)
$(A_{42}/A_{31})\,[(I_B/I_A) - (A_{32}/A_{31})]^{-1}$ (□)
$\sqrt{T}/P$ ($K^{1/2}$/mTorr)

Figure II.4. A plot of the left-hand sides of Eqs. (II.18) and (II.19) against $\sqrt{T}/P$, illustrating Rb*-Rb f.s. mixing of the 7^2D states. The error bars are representative of experimental error over the Rb-density range.

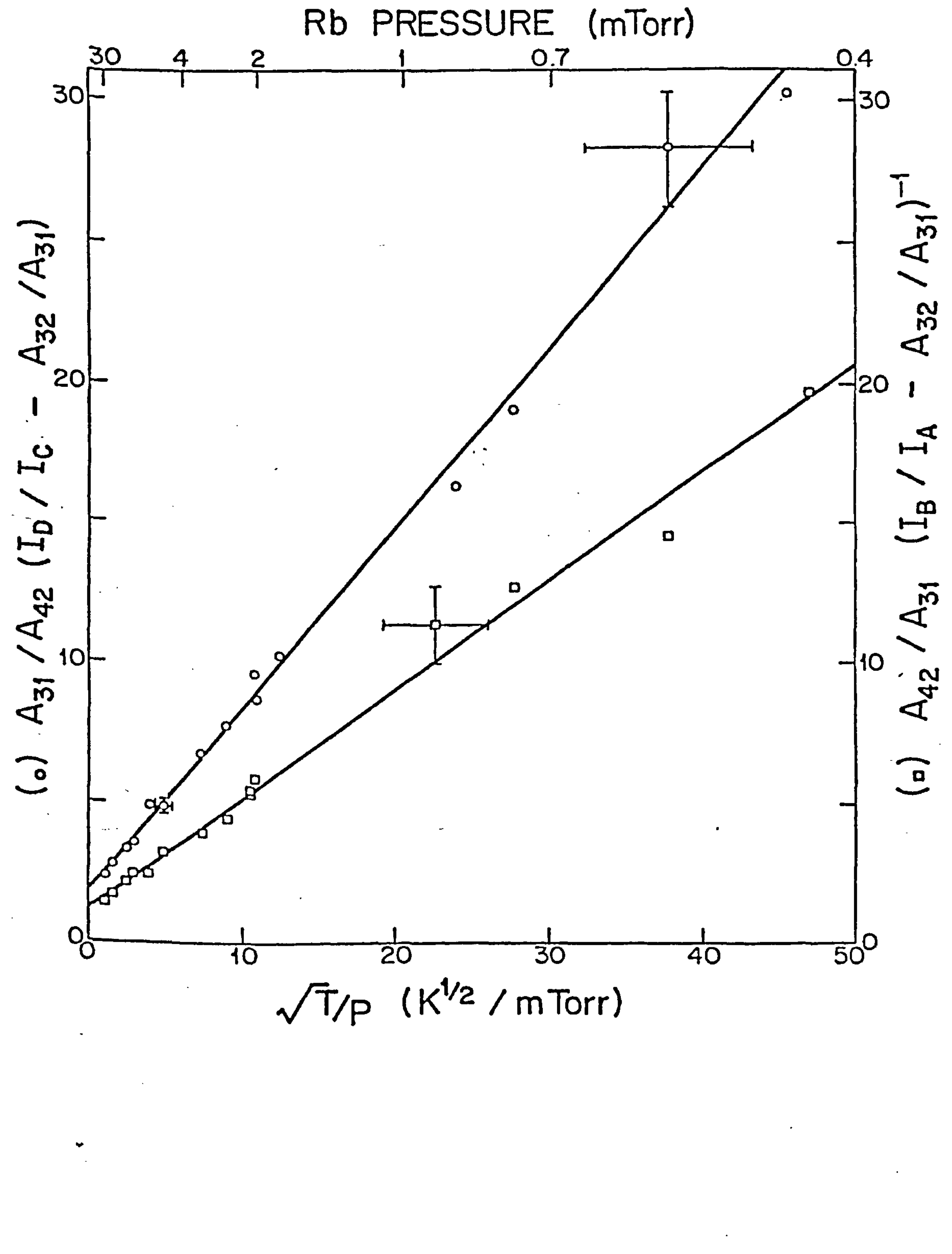
Rb PRESSURE (mTorr)
30
4
2
1
0.7
0.4
(○) A_{31}/A_{42} (I_D/I_C - A_{32}/A_{31})
(□) A_{42}/A_{31} (I_B/I_A - A_{32}/A_{31})$^{-1}$
0
10
20
30
40
50
$\sqrt{T}/P$ ($K^{1/2}$ / mTorr)

Figure II.5. A plot of the left-hand sides of Eqs. (II.18) and (II.19) against $\sqrt{T}/P$, illustrating Rb^*-Rb f.s. mixing of the 8^2D states. The error bars are representative of experimental error over the Rb-density range.

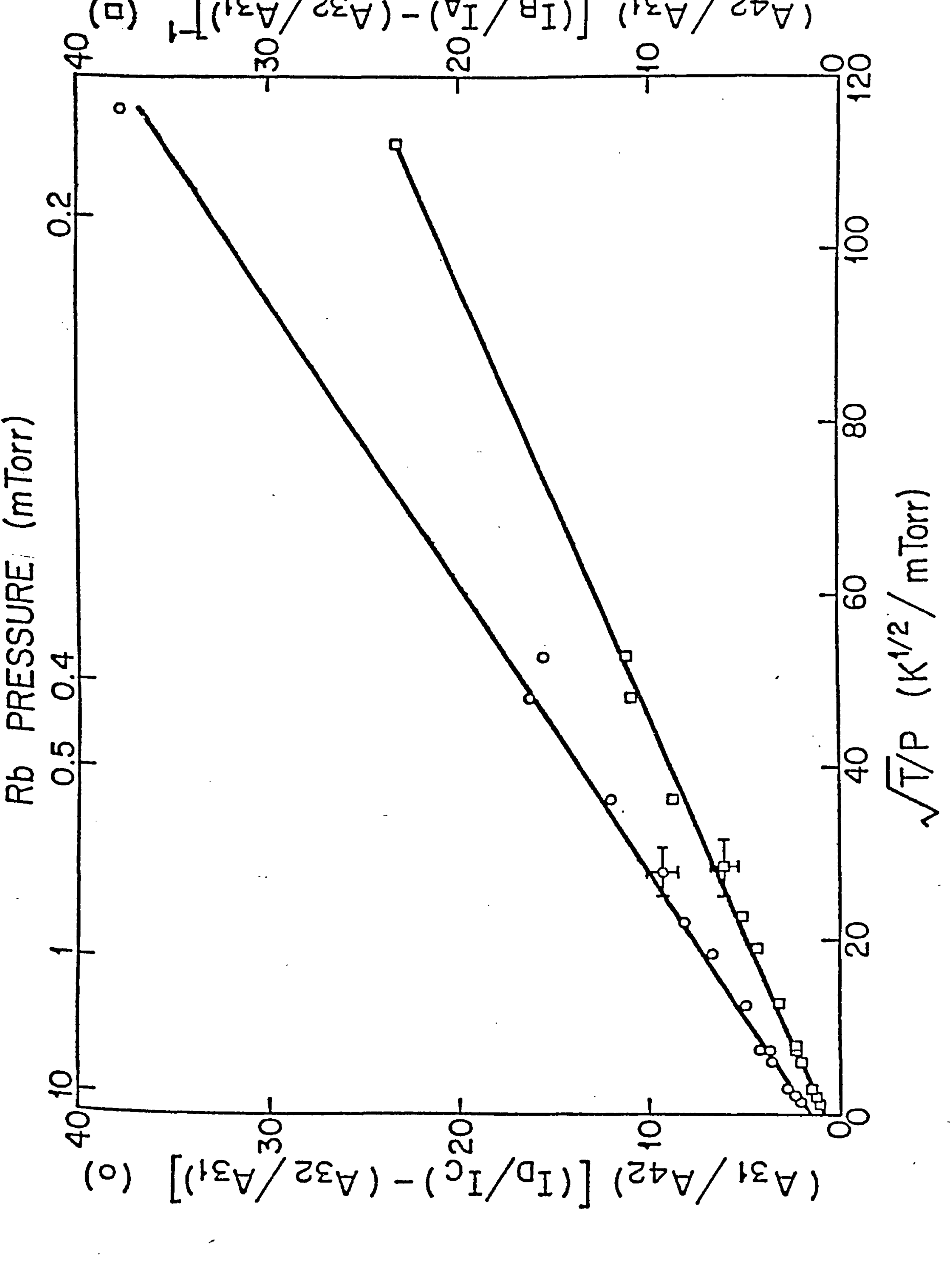
Rb PRESSURE (mTorr)
10
1
0.5
0.4
0.2
$\sqrt{T/P}$ $(K^{1/2}/mTorr)$
0
20
40
60
80
100
120
$(A_{31}/A_{42})\,[(I_D/I_C) - (A_{32}/A_{31})]$ (○)
0
10
20
30
40
$(A_{42}/A_{31})\,[(I_B/I_A) - (A_{32}/A_{31})]^{-1}$ (□)
0
10
20
30
40

from errors in the Einstein A coefficients.

The cross sections for Rb*-Rb collisions are listed in Table II.5, together with other results recently reported in the literature. It is apparent that, for any particular fine-structure transition, some of the reported cross sections differ appreciably from one another, depending on the method employed, though there is agreement within an order of magnitude. The cross sections for $n = 5 - 9$, measured by Parker et al. (1984), appear to vary in a regular manner with n^*, the effective principal quantum number of the excited state. In the absence of theoretical calculations the cross sections can only be compared with σ_g, the geometrical cross sections, which are also shown in Table II.5. The behaviour of the experimentally determined cross sections in this region of n^* is qualitatively similar to variation of σ_g with n^* and the values of the two kinds of cross sections are also comparable; these features were noted by Hugon et al. (1980b) who measured the cross sections for collisional transfer out of the $n^2D_{3/2}$ Rb states (for $9 \leqslant n \leqslant 13$) to all other quantum states including the other f.s. sublevel ($n^2D_{5/2}$). Hugon's cross sections may therefore be considered approximately equivalent to the sum of my $Q_{34}+Q_3$. Very large cross sections for resonant alkali-alkali collisions, even exceeding σ_g, are not unusual, bearing in mind that the interaction takes place between the "quasi-free" valence electron of the excited atom and the ground-state Rb atom,

TABLE II.5.

Cross Sections for $^2D_{3/2} \leftrightarrow {}^2D_{5/2}$ Mixing Induced in Rb* - Rb Collisions

Excited State	FS Splitting (cm^{-1})	$Q_{34}(D_{3/2} \rightarrow D_{5/2})$ ($10^{-14} cm^2$)	$Q_{43}(D_{5/2} \rightarrow D_{3/2})$ ($10^{-14} cm^2$)	$Q_{34}:Q_{43}$	Q_3 ($10^{-14} cm^2$)	Q_4 ($10^{-14} cm^2$)	n*	σ_g ($10^{-14} cm^2$)
5^2D	2.96		2.9 ± 0.6a)				3.71	3.14
6^2D	2.26		10 ± 6b)				4.68	8.90
6^2D	2.26		6.9 ± 1.4a)				4.68	8.90
6^2D	2.26	17.3 ± 3.5c)	11.6 ± 2.3c)	1.49c)	8 ± 4c)	4 ± 3c)	4.68	8.90
7^2D	1.51		11.5 ± 2.3a)				5.67	20.3
7^2D	1.51	30 ± 5c)	18 ± 3c)	1.65c)	19 ± 6c)	7 ± 2c)	5.67	20.3
8^2D	1.01		17.1 ± 3.0a)				6.67	40.2
8^2D	1.01	43.1 ± 8.6c)	28.5 ± 8.6c)	1.51c)	8 ± 6c)	7 ± 5c)	6.67	40.2
8^2D	1.01	81 ± 16d)	55 ± 11d)	1.47d)	35 ± 22d)	28 ± 29c)	6.67	40.2
9^2D	0.70		26.0 ± 5.0a)				7.66	71.3
9^2D	0.70	70 ± 30e)				8 ± 3e)	7.66	71.3

a) Parker et al. (1984).

b) Hill et al. (1982).

c) This investigation

d) Głódź et al. (1981).

e) Gounand et al. (1979).

and is governed by long-range forces due to the generally large polarizability of the ground-state alkali (and in particular Rb) atoms (Omont 1977).

The experimental values of Głódź et al. (1981) appear to be too large, probably because they used a sealed fluorescence cell in their experiment. The cell walls, in spite of the usual baking treatment, are always a source of gaseous contaminants which tend to perturb the fluorescence intensity measurements, particularly at the very low pressures in the mtorr region. I have found this effect to be quite significant; even when the stopcock on the cell was kept closed for about 1 h, there was already a change in the measured fluorescent intensity ratio at a constant (low) buffer-gas pressure. The discrepancies with the cross sections reported by Parker et al. (1984) are more difficult to explain. In their calculations these authors used slightly different values of the Einstein A coefficients and much different lifetimes of the Rb ^2D states than those used here. At the time when I began this series of experiments, the lifetimes derived from the calculations of Anderson and Zilitis (1964) were the most reliable because of their agreement with the experimental data of Lundberg and Svanberg (1976). More recent experimental (Marek and Münster 1980) and theoretical (Theodosiou 1984) investigations suggest, however, that the lifetimes for the relevant ^2D states are lower than those obtained using oscillator strengths derived by Anderson and

Zilitis (1964). Table II.6 lists the values of lifetimes reported by the various authors.

TABLE II.6. Lifetimes of n^2D Rb states from various sources (ns)

n	Ref. a	Ref. b	Ref. c	Ref. d
6	313	285±16	237±15	245
7	397	388±25	325±22	318
8	538	515±30	421±25	430

a) Anderson and Zilitis (1964), theoretical

b) Lundberg and Svanberg (1976), experimental

c) Marek and Münster (1980), experimental

d) Theodosiou (1984), theoretical

Parker et al. (1984) used Marek and Münster's results which are equal to those quoted by Theodosiou within experimental error. The lifetimes used in this investigation to calculate the cross sections are therefore about 20-25% longer than the values used by Parker et al. If I used Theodosiou's lifetimes instead, my cross sections would be increased by 20-25%, which would cause the divergencies between my results and those of Parker et al. (1984) to become even larger. In trying to find a rational explanation for these differences it should be considered that, while the 6^2D mixing cross section is quoted by

Parker et al. (1984) to be 6.9×10^{-14} cm^2, the corresponding cross section for Rb^*-Xe collisions measured in the same laboratory (Zollars et al. 1983) is reported as 9.3×10^{-14} cm^2. In all known cases the alkali-alkali fine-structure mixing cross section is larger than the corresponding alkali-noble gas cross section because of the already mentioned much larger polarizability of the alkali atom (Omont 1977) implying stronger interaction (Wolnikowski et al. 1982; Supronowicz et al. 1984). The contrary indication given by Parker et al. (1984) and Zollars et al. (1983) poses the question whether the authors may not have overestimated the Rb vapour density in their system, especially since the ratio Q_{43}(my results):Q_{43}(Schuessler's group's results) is constant for the 6^2D, 7^2D and 8^2D states within the stated limits of error. It should be borne in mind that the parameter which is actually measured in experiments dealing with thermal collisions, is the product $Q\tau N_0$ and, consequently, the accuracy of the resulting cross sections Q cannot be higher than the accuracy of the lifetime τ and density N_0 of the collision partners. There is, therefore, agreement between the relative though not absolute values of the two sets of cross sections. The effective cross sections for quenching (out of the fine-structure doublet) are smaller than the mixing cross sections, since the particular Rb D states are distant from other states (Hugon et al. 1980b).

Various other possible sources of systematic error were considered and are deemed to be negligible. The effects of saturation, photoionization and pooling collisions were all studied by measuring the intensities of the two fluorescent components in relation to laser power. At low laser powers, typical of the conditions under which the data were taken, the intensities varied quadratically with laser power as expected for two-photon excitation, and the intensity ratio of sensitized-to-direct fluorescence remained constant, indicating that pooling collisions and photoionization were not significantly affecting the results. The intensities and intensity ratios deviated from this behaviour only at much higher laser powers.

Collisions with Rb_2 molecules whose density was lower than the Rb density by 3 orders of magnitude (Nesmeyanov 1963), would contribute negligibly to the observed effects, as would three-body collisions at the prevailing vapour densities. Black-body radiation-stimulated transitions (Cooke and Gallagher 1980) would cause an increase in the depopulation rate or an effective decrease in the ^2D lifetimes which, however, amounts to less than 3% of the calculated lifetimes (Farley and Wing 1981) and can thus be neglected. I have also rejected the possibility of collisions with the cell walls since the fluorescing region was located at the center of the cell which was 2.5 cm in diameter and the excited Rb atoms could travel only about 2 mm during the time of observation, even in the absence of any collisions.

The experimental data representing 6^2D, 7^2D and 8^2D fine-structure mixing by buffer gases, shown graphically in Figs. II.6-II.10, are listed in Tables II.7, II.8 and II.9. Table II.7 also shows the 6^2D cross sections reported by Zollars et al. (1983). Here the graphs are also linear, except for some slight departures from linearity at low pressures of Ne and Ar (for n=7), which are due to the previously mentioned difficulties with the McLeod gauge in this pressure region (only the linear data were used for calculations). It might be noted that the scatter of the data points corresponding to the I_B/I_A ratios is noticeably larger than the scatter of the I_D/I_C points, particularly at the lowest buffer-gas (or Rb-vapour) pressures. When $^2D_{3/2}$ is the optically excited state, the B fluorescent component consists of a mixture of direct and collisionally sensitized fluorescence and, in order that the semsitized fluorescent intensity component be determined with good accuracy, its intensity should be comparable to the intensity of the direct fluorescence. This is accomplished only when the buffer-gas pressure exceeds some lower limit; otherwise, the experimental value of the point on the graph, representing the left-hand side of Eq. (II.18), becomes very sensitive to the intercalibration of the two photon-counting channels and even a small error in their relative sensitivity results in considerable scatter of the measured intensity ratios.

Tables II.7-9 also quote the quenching cross sections

Figure II.6. Plots of the left-hand sides of Eqs. (II.18) and (II.19) against $\sqrt{T}/P$ for He, Ne, Ar, Kr, and N_2, illustrating 6^2D fine-structure mixing. Rough values of gas pressures are indicated along the abscissa. The error bars are representative of experimental error over the range of gas densities.

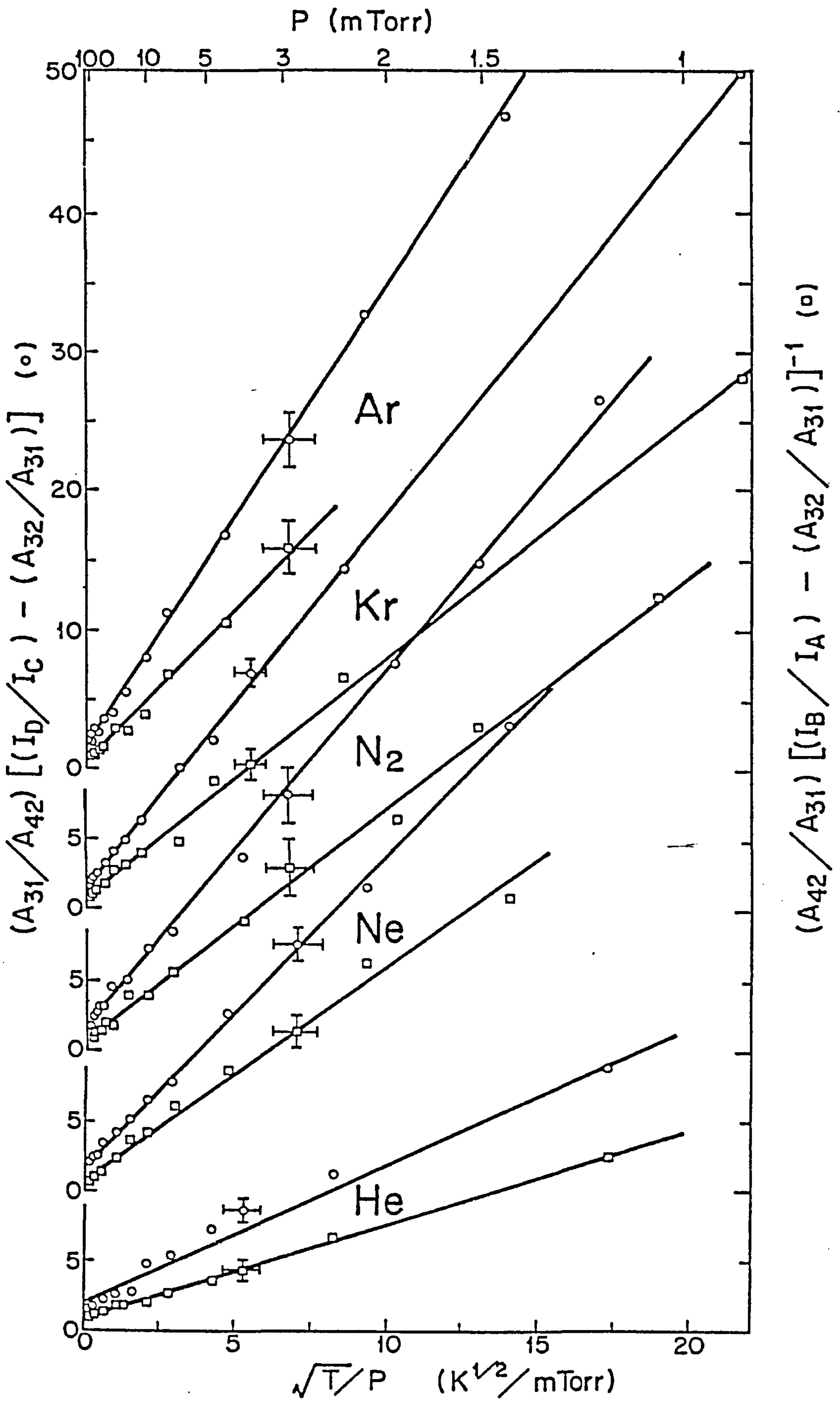
P (mTorr)
100
10
5
3
2
1.5
1
50
40
30
20
10
0
5
0
5
0
5
0
5
0
Ar
Kr
N2
Ne
He
$(A_{31}/A_{42})\,[(I_D/I_C) - (A_{32}/A_{31})]$ (○)
$(A_{42}/A_{31})\,[(I_B/I_A) - (A_{32}/A_{31})]^{-1}$ (□)
0
5
10
15
20
$\sqrt{T}/P$ $(K^{1/2}/\mathrm{mTorr})$

Figure II.7. Plots of the left-hand sides of Eqs. (II.18) and (II.19) against $\sqrt{T}/P$ for He, Ne, and Ar, showing 7^2D mixing and quenching. The error bars are representative of experimental error over the range of noble-gas densities.

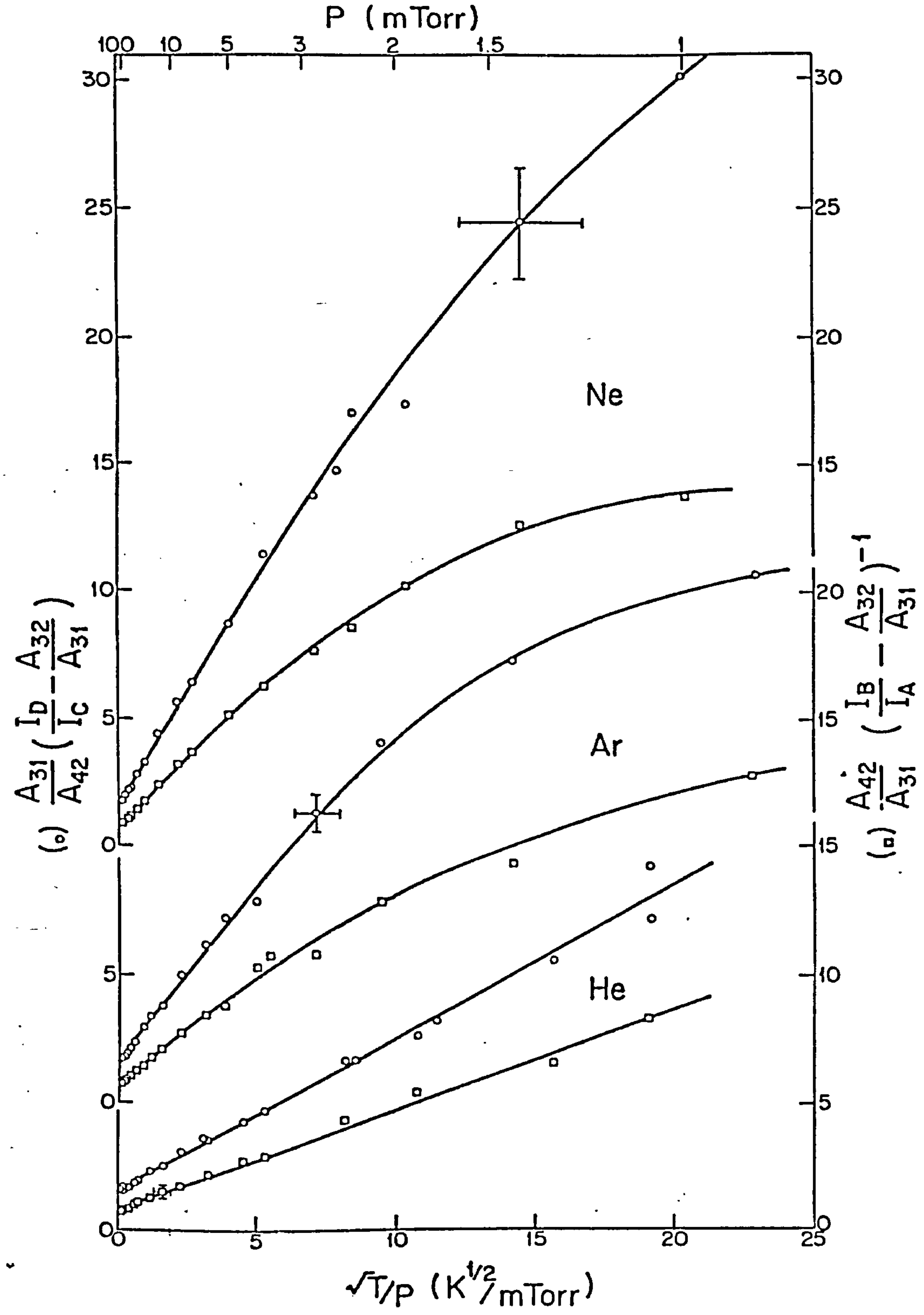
P (mTorr)
100
10
5
3
2
1.5
1
30
25
20
15
10
5
0
5
0
0
Ne
Ar
He
(∘) $\frac{A_{31}}{A_{42}}\left(\frac{I_D}{I_C}-\frac{A_{32}}{A_{31}}\right)$
(▫) $\frac{A_{42}}{A_{31}}\left(\frac{I_B}{I_A}-\frac{A_{32}}{A_{31}}\right)^{-1}$
30
25
20
15
20
15
10
5
0
0
5
10
15
20
25
$\sqrt{T}/P$ ($K^{1/2}$/mTorr)

Figure II.8. Plots of the left-hand sides of Eqs. (II.18) and (II.19) against $\sqrt{T}/P$ for Kr, Xe, and N_2, showing 7^2D mixing and quenching. The error bars are representative of experimental error over the range of gas densities.

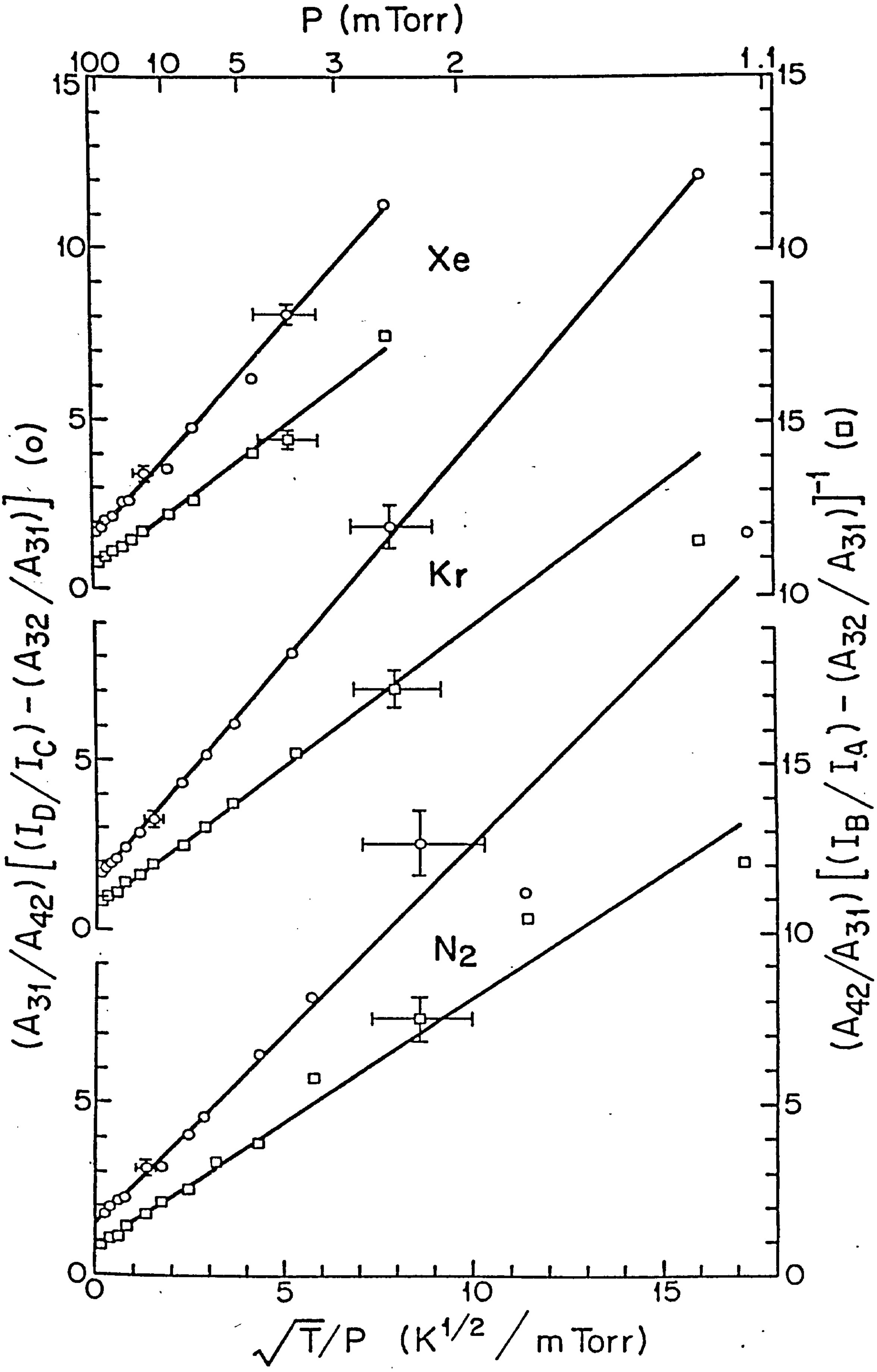
P (m Torr)
100
10
5
3
2
1.1
15
10
5
0
Xe
Kr
N2
$(A_{31}/A_{42})[(I_D/I_C)-(A_{32}/A_{31})]$ (o)
$(A_{42}/A_{31})[(I_B/I_A)-(A_{32}/A_{31})]^{-1}$ (□)
$\sqrt{T}/P$ ($K^{1/2}$ / m Torr)
0
5
10
15

Figure II.9. Plots of the left-hand sides of Eqs. (II.18) and (II.19) against $\sqrt{T}/P$ for He, Ne, and Ar, showing 8^2D mixing and quenching. The error bars are representative of experimental error over the range of noble-gas densities.

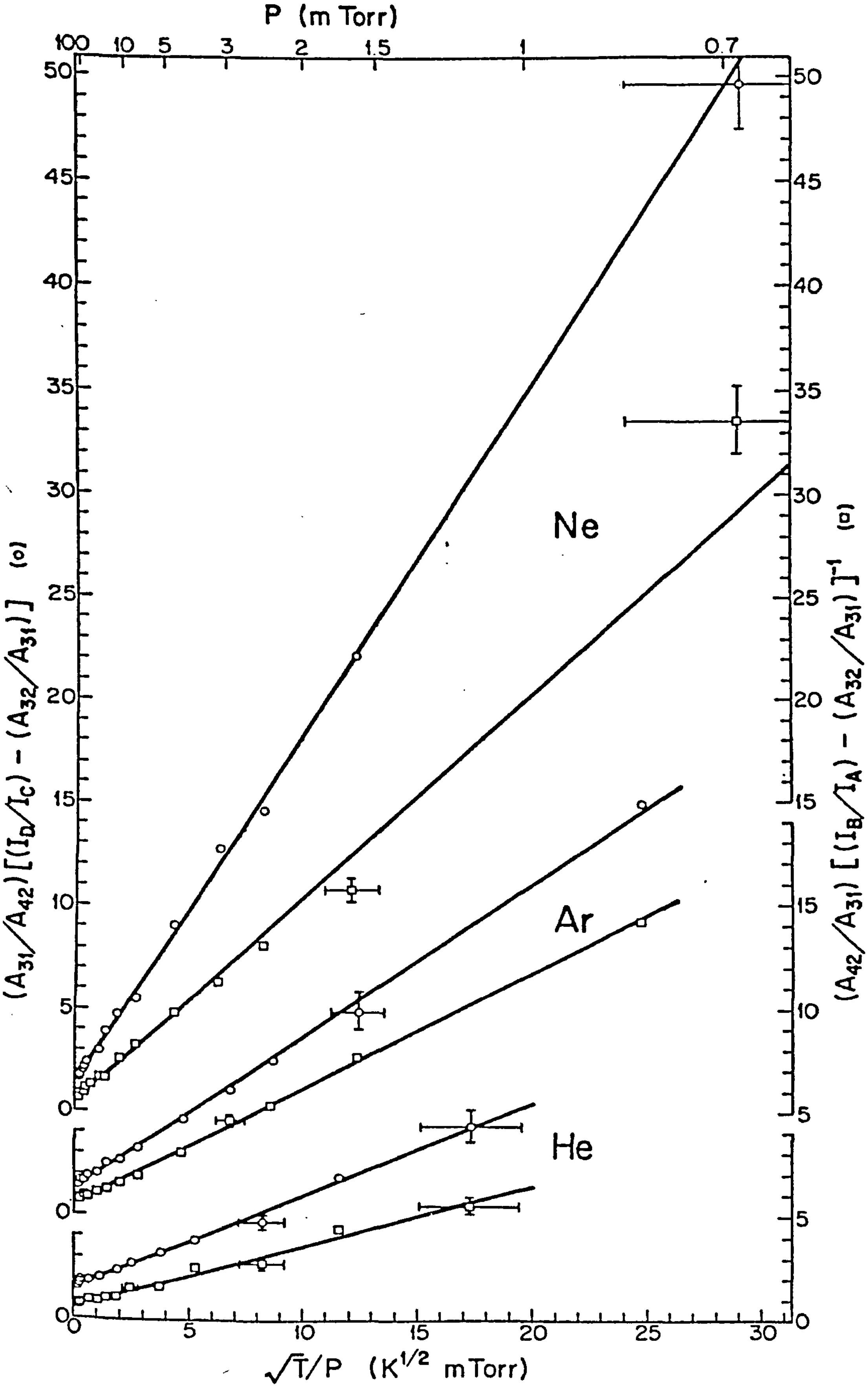
P (m Torr)
100
10
5
3
2
1.5
1
0.7
50
45
40
35
30
25
20
15
10
5
0
0
0
Ne
Ar
He
$(A_{31}/A_{42})[(I_D/I_C) - (A_{32}/A_{31})]$ (o)
$(A_{42}/A_{31})[(I_B/I_A) - (A_{32}/A_{31})]^{-1}$ (□)
5
10
15
20
25
30
$\sqrt{T}/P$ ($K^{1/2}$ mTorr)

Figure II.10. Plots of the left-hand sides of Eqs. (II.18) and (II.19) against $\sqrt{T}/P$ for Kr, Xe, and N_2, showing 8^2D mixing and quenching. The error bars are representative of experimental error over the range of gas densities.

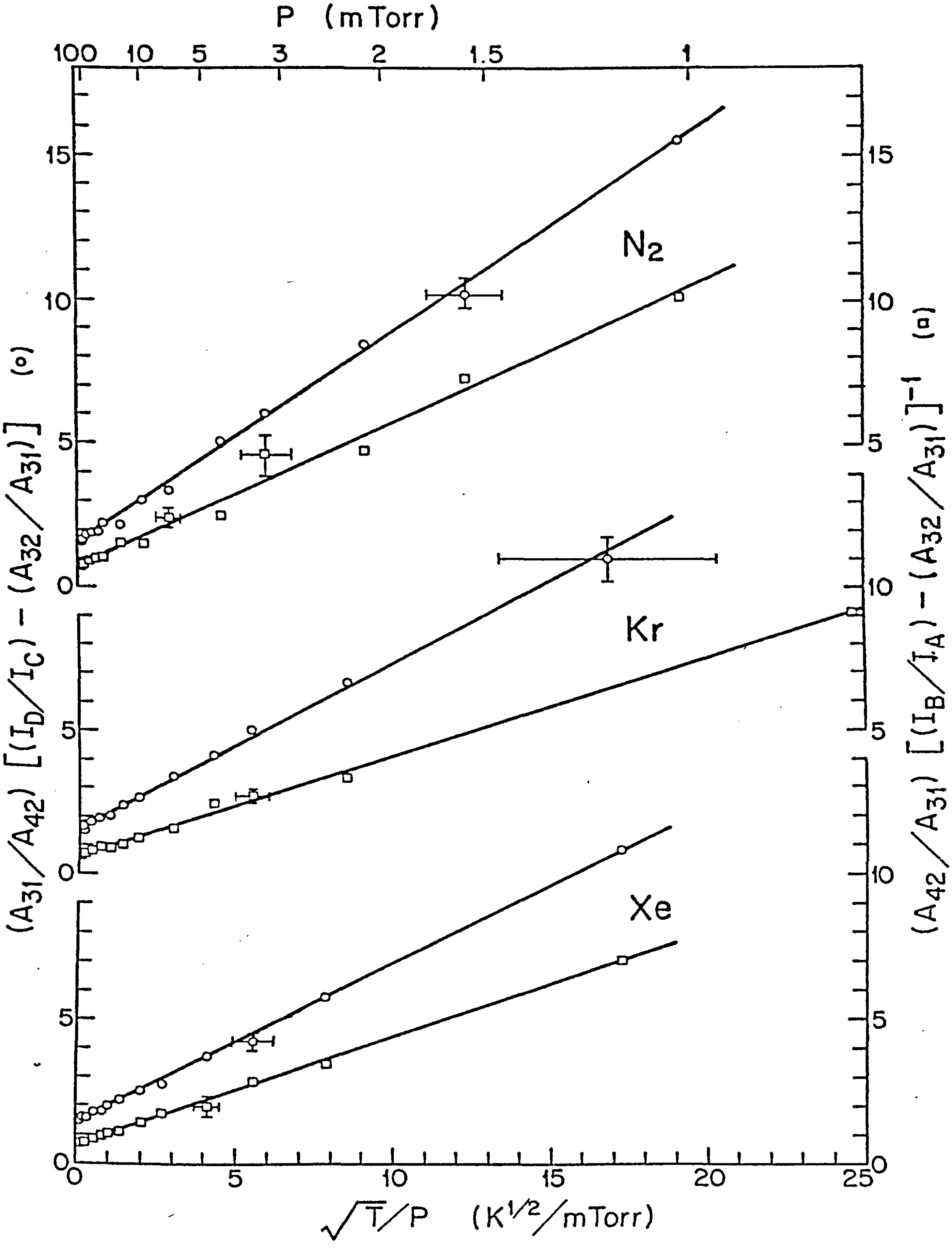
P (m Torr)
100
10
5
3
2
1.5
1
N2
Kr
Xe
$(A_{31}/A_{42})\,[(I_D/I_C) - (A_{32}/A_{31})]$ (o)
$(A_{42}/A_{31})\,[(I_B/I_A) - (A_{32}/A_{31})]^{-1}$ (□)
0
5
10
15
20
25
$\sqrt{T}/P$ ($K^{1/2}$/mTorr)

TABLE II.7.

Cross Sections for $6^2D_{3/2} \leftrightarrow 6^2D_{5/2}$ Mixing in Rb Induced in Collisions with Buffer Gases

Collision Partners	$Q_{34}(D_{3/2} \rightarrow D_{5/2})$ (10^{-14} cm^2)	$Q_{43}(D_{5/2} \rightarrow D_{3/2})$ (10^{-14} cm^2)	Q_{34}/Q_{43}	$Q_3(^2D_{3/2})$ (10^{-14} cm^2)	$Q_4(^2D_{5/2})$ (10^{-14} cm^2)
Rb-He	6.6 ± 1.0	4.5 ± 0.7	1.47	0.0 ± 0.4	0.4 ± 0.3
Rb-He[a)]		2.4 ± 0.9			
Rb-Ne	6.1 ± 0.9	4.1 ± 0.6	1.48	0.7 ± 0.7	0.0 ± 0.5
Rb-Ne[a)]		3.1 ± 1.2			
Rb-Ar	5.3 ± 0.8	3.6 ± 0.6	1.48	0.5 ± 0.6	0.0 ± 0.2
Rb-Ar[a)]		2.6 ± 1.0			
Rb-Kr	8.5 ± 1.3	5.5 ± 0.8	1.55	0.2 ± 0.3	0.5 ± 0.4
Rb-Kr[a)]		5.8 ± 2.2			
Rb-Xe[a)]		9.3 ± 5.6			
Rb-N_2	6.4 ± 1.0	4.1 ± 0.6	1.56	0.7 ± 0.7	0.5 ± 0.5

a) Zollars et al. (1984).

TABLE II.8.

Cross Sections for $7^2D_{3/2} - 7^2D_{5/2}$ Mixing in Rb Induced in Collisions with Buffer Gases

Collision Partners	$Q_{34}(D_{3/2} \rightarrow D_{5/2})$ $(10^{-14} cm^2)$	$Q_{43}(D_{5/2} \rightarrow D_{3/2})$ $(10^{-14} cm^2)$	Q_{34}/Q_{43}	$Q_3(^2D_{3/2})$ $(10^{-14} cm^2)$	$Q_4(D_{5/2})$ $(10^{-14} cm^2)$	Q Theor. $(10^{-14} cm^2)$
Rb-He	8.8 ± 1.3	5.8 ± 0.9	1.51	1.1 ± 0.3	0.3 ± 0.1	7.5[a)]
Rb-Ne	6.5 ± 1.0	4.0 ± 0.6	1.62	0.2 ± 0.1	0.2 ± 0.1	
Rb-Ar	10.4 ± 1.6	6.9 ± 1.0	1.50	0.1 ± 0.1	0.5 ± 0.5	10[a)]
Rb-Kr	14.1 ± 1.5	9.0 ± 1.0	1.57	0.3 ± 0.2	0.2 ± 0.2	
Rb-Xe	15.5 ± 2.0	10.5 ± 1.5	1.48	0.7 ± 0.4	0.4 ± 0.3	
Rb-N_2	10.0 ± 1.5	6.9 ± 1.0	1.45	0.8 ± 0.4	0.3 ± 0.3	

a) Hahn (1981).

TABLE II.9.

Cross Sections for $8^2D_{3/2} \leftrightarrow 8^2D_{5/2}$ Mixing in Rb induced in Collisions with Buffer Gases

Collision Partners	$Q_{34}(D_{3/2} \rightarrow D_{5/2})$ $(10^{-14} cm^2)$	$Q_{43}(D_{5/2} \rightarrow D_{3/2})$ $(10^{-14} cm^2)$	Q_{34}/Q_{43}	$Q_3(^2D_{3/2})$ $(10^{-14} cm^2)$	$Q_4(^2D_{5/2})$ $(10^{-14} cm^2)$	Q Theor. $(10^{-14} cm^2)$
Rb-He	8.9 ± 1.4	5.8 ± 0.9	1.51	0.3 ± 0.3	0.4 ± 0.3	8 a)
Rb-Ne	4.9 ± 1.0	3.2 ± 0.6	1.53	0.2 ± 0.2	0.2 ± 0.2	
Rb-Ar	12.4 ± 2.5	9.4 ± 1.9	1.32	0.7 ± 0.7	0.5 ± 0.5	12.5 a)
Rb-Kr	24.9 ± 5.0	15.1 ± 3.0	1.65	0.7 ± 0.8	0.8 ± 1.0	
Rb-Xe	25.8 ± 3.9	17.6 ± 2.7	1.47	0.3 ± 0.5	0.2 ± 0.5	
$Rb-N_2$	12.1 ± 2.4	8.3 ± 1.7	1.46	0.7 ± 0.6	0.3 ± 0.4	

a) Hahn (1981).

which, however, should be regarded as a by-product of the experiment since they were determined indirectly using the mixing cross sections and may, at best, be accurate within an order of magnitude. The various sources of experimental error have already been mentioned in connection with the Rb^*-Rb collisions; in the present case the uncertainty in Rb density as determined from the temperature - vapour pressure relation (Nesmeyanov 1963), is of no particular importance, though there is a possibility of the results being inflated through the contribution of Rb^*-Rb collisions to the ^2D mixing process. At Rb vapour densities of 1×10^{12} cm^{-3} which were employed in these experiments I found that, in the most unfavourable case, the necessary correction to the measured fluorescent intensity ratios did not exceed 5%. The error assigned to the values of Q_{43} and Q_{34} for collisions of Rb with various gases was $\pm$10 - 20%, depending on the scatter of the data points.

The cross sections listed in Tables II.7-II.9 are significantly smaller than the cross sections for Rb^*-Rb collisions in which the interaction has a much longer range. The noble-gas cross sections exhibit a relative ordering from He to Kr with a minimum at Ar for n=6 and at Ne for n=7,8, which correlates with the elastic electron - noble-gas scattering cross section. This effect can be interpreted as being due to at least three different trends in the cross-sections; this accounts for the fact that no simple theoretical model works well in the range of "intermediate" excited states.

(i) The interaction of the "quasi-free" valence electron of the excited rubidium atom with the perturber particle is weakest for Ne and Ar. However, the "quasi-free" electron model is limited to higher-excited states, except perhaps for the case of Ne, where the range of the principal quantum number n (n=6,7,8) lies at the limit of the model's applicability (Omont 1977). Based on this trend alone, the ordering of the mixing cross section should not be expected to follow closely the elastic electron scattering cross sections.

(ii) The velocity dependence of the alkali-noble gas mixing cross sections is such, that in the range of relatively low (thermal) velocities of the colliding partners the cross sections increase rather quickly with the velocity of the partners' relative motion, as the character of a collision changes from "adiabatic" to "sudden" (Callaway and Bauer 1965; Gallagher 1968). This experiment was performed under conditions of thermal equilibrium and the fluorescence cell was maintained at the same temperature during all the measurements with the buffer gases, and, accordingly, the cross sections should tend to increase with the relative velocity of the colliding partners (and thus decrease with the atomic mass of the noble gas atom, i.e. from He to Xe).

(iii) An opposite trend can be inferred from the fact, that the polarizabilities of the noble gases increase from He to Xe (Dalgarno and Kingston 1960). Even when the perturber particle is spherically symmetric, there is still some remaining long-range electrostatic interaction between the perturber particle and the ionic core of an excited atom (Fermi 1934). Since this interaction is proportional to the polarizability of the perturber, one can expect that larger polarizabilities will result in larger cross sections.

It is not obvious, which of these mechanisms predominates in producing the relative ordering of the fine-structure mixing cross sections. However, it is likely that the same mechanism governs the various inelastic collisional processes involving alkali atoms in this "intermediate" region of n. Similar ordering, which has been observed in studies of collisional l-mixing in sodium (Gallagher et al. 1977) and even in ^2P mixing between alkali resonance fine-structure states (Krause 1975; Ciuryło and Krause 1982), where the valence electron would be expected to be more tightly bound, is not apparent in the results of Zollars et al. (1983). This is illustrated in Figs. II.11 and II.12. The values of velocity-dependent electron cross sections (Massey and Burhop 1952) were taken to correspond to the orbital velocities of the 6D, 7D or 8D valence electrons, calculated according to Jefimenko's model (Jefimenko 1963) and using a covalent Rb ground-state atomic radius r=2.11 Å given by Coulson (1958). Figures II.11-II.12 show how the mixing cross sections and

Figure II.11. Variation of cross sections Q_{43} for Rb - noble gas collisions with the atomic numbers of the noble gases, compared with a similar variation of the elastic electron scattering cross section σ. ◇, this investigation; ⊡, Zollars et al. (1983); □, corresponding to the 6D orbital electron velocity. The curve indicates the trend of the σ cross sections. No physical dependence of cross section on atomic number is implied.

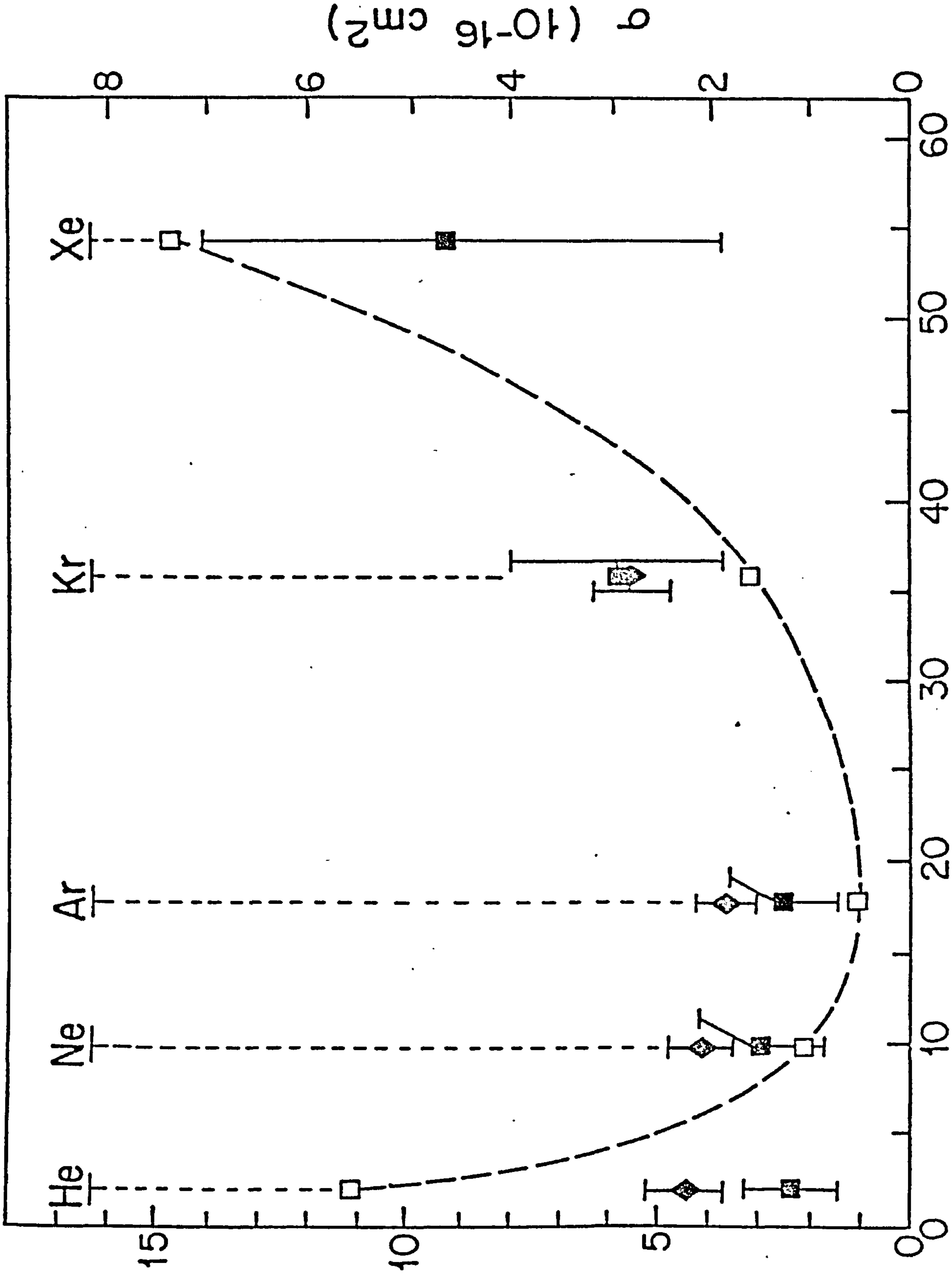
He
Ne
Ar
Kr
Xe
ATOMIC NUMBER
0
10
20
30
40
50
60
Q43 (10-14 cm2)
0
5
10
15
σ (10-16 cm2)
0
2
4
6
8

Figure II.12. Variations of cross sections Q_{43} for Rb - noble-gas collisions with the atomic number of the noble gases, compared with similar variations of the elastic electron scattering cross sections σ. ▲ and ● represent Q_{43} for 7^2D and 8^2D states, respectively. △ and ○ represent σ corresponding to the orbital velocities of the respective ^2D electrons.

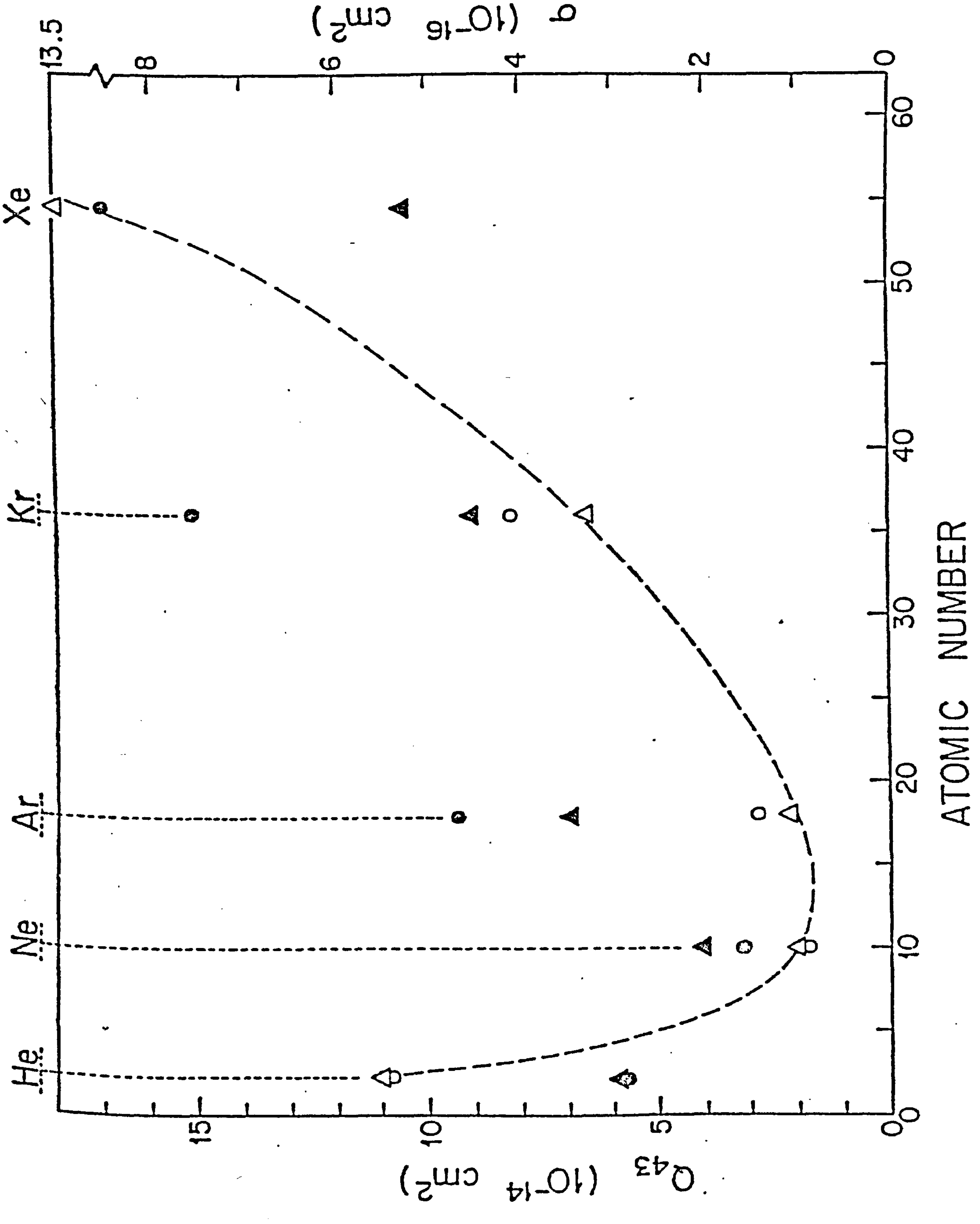
He
Ne
Ar
Kr
Xe
ATOMIC NUMBER
0
10
20
30
40
50
60
Q_{43} (10^{-14} cm^2)
0
5
10
15
σ (10^{-16} cm^2)
0
2
4
6
8
13.5

the elastic electron scattering cross sections vary from one noble gas to the other. It may be seen that the cross sections σ, corresponding to the 6D, 7D and 8D electrons, all follow similar trends. In each case the cross section for He is larger than for Ne or Ar, and there is a minimum in the vicinity of Ar for n=6 and Ne for n=7,8; the behaviour is thus identical with that of the mixing cross sections, even though the latter are larger than σ by 1 to 2 orders of magnitude (it should be borne in mind that the cross sections σ are only the relative measures of the strength of interaction between a free electron and a noble-gas atom and therefore they need not be of a size equal to the mixing cross sections). The apparently different ordering of Zollars' (1983) cross sections might well be due to the effects of gaseous impurities adsorbed on the sealed cell which was used in their experiment, particularly at the extremely low noble-gas pressures.

It might be noted that, as the principal quantum number increases from 6 to 8, the variation of the mixing cross sections from He to Xe becomes more accentuated. This is in accord with the semiclassical model put forward by Omont (1977) according to which, for smaller n (high density of the electronic cloud of the excited Rb atom), the collisions are of the 'strong' type and the excitation transfer is induced by a collision with a probability close to 100% for all the noble gases, while for larger n the probability of excitation transfer is smaller, the collision is 'weak' and the cross sections vary from one noble gas to another (as does σ, the electron scattering cross section). In the present case the full criterion for a weak collision was never quite fulfilled and was most closely approached in the case of n=8 and Ne as collision partner. The phenomenon of decreasing cross sections with increasing n can be seen only for Ne which, of all the noble gases, appears to interact most weakly with Rb. For other noble gases this effect is expected at higher n values (Hahn 1981; de Prunelé and Pascale 1979) where Omont's criterion for a 'weak collision' is satisfied and the cross sections vary significantly from one noble gas to another, following more closely the variations of the elastic electron scattering cross-sections (Omont 1977).

While for very large n all cross sections are expected to decrease with n, this is not necessarily true for intermediate n values. Experiments on collisional mixing in Na (Gallagher et al. 1977) and quenching of F-states in Rb (Hugon et al. 1979) indicate that at low n the cross sections tend to rise with n, reach a maximum and gradually decrease at larger n. The value of n corresponding to the maximum depends on the particular noble gas. As may be seen in Tables II.7-9, in the case of the ^2D Rb states, the cross sections increase with n for Ar, Kr and Xe. As was already pointed out, for Ne the cross sections decrease with n while for He the 7^2D and 8^2D cross sections are equal, perhaps indicating that a maximum has been reached;

for the heavier gases, Ar and, especially, Kr and Xe, a maximum in the cross sections is expected at higher n values (de Prunelé and Pascale 1979; Hahn 1981).

Although most theoretical studies of inelastic transfer cross sections for alkali atoms apply either to the resonance states or to much more highly excited Rydberg states, a useful comparison of the data for He and Ar (for n=7 and 8) can be made with Hahn's (1981) calculations. As shown in Tables II.8, II.9, a slight extrapolation of his curves describing the n-dependence of the cross sections produces values in good agreement with my experimental results.

Tables II.7-II.9 also include mixing and quenching cross sections for collisions with N_2. No theoretical treatments of these interactions have been reported in the literature, even though de Prunelé and Pascale (1979) attempted to calculate the cross sections for quenching of Na ^2D states by N_2 collisions. Their model, however, is applicable to more highly excited (Rydberg) states and produces agreement with experimental measurements only for n>10. In the present case it is apparent that the cross sections for 7^2D and 8^2D mixing by N_2 are equal to the Ar cross sections, and for 6^2D they are only slightly higher; the respective quenching cross sections are also equal within experimental error. The equality of the mixing cross sections for N_2 and Ar is not surprising. The ^2D fine-structure splittings are very much smaller than the rotational energy spacing in N_2 and thus the rotational (and vibrational) molecular degrees of freedom cannot participate in the inelastic process which otherwise would be enhanced by such a quasiresonance (Hrycyshyn and Krause 1970; Cuvellier et al. 1983). Accordingly, since N_2 and Ar have nearly equal masses and polarizabilities, the cross sections, too, are similar. It is less obvious why the quenching cross sections should be equally similar, though the values are so inaccurate that they actually might differ by an order of magnitude. It is likely that the depopulation of the ^2D states takes place through transfer to intermediate lower-lying states, accompanied by radiative cascades, since a direct radiationless transfer to the ground state could not very well be effected by a collision with a noble-gas atom as it would involve the conversion of a large amount of excitation energy into kinetic energy of relative motion (Krause 1975). On the other hand, the N_2 quenching cross sections which lie in the range 10-100 $\AA$, are close in magnitude to similar cross sections for quenching of intermediate n^2P states in Rb (Siara and Krause 1973) and Cs (Siara et al. 1982), and nS ($5 \leqslant n \leqslant 9$) states in Na (Humphrey et al. 1978).

According to the principle of detailed balancing, the mixing cross sections should be in the ratio

$$Q_{34}/Q_{43} = (g_4/g_3)\exp(-\Delta E/kT), \qquad \text{(II.20)}$$

where $g_4=6$ and $g_3=4$ are the statistical weights ($g=2J+1$) of the $^2D_{5/2}$ and $^2D_{3/2}$ states, respectively, and ΔE is the n^2D fine-structure splitting for the appropriate n. For n=6,7 or 8 and cell temperatures of about 380 K, Eq. (II.20) predicts $1.49<Q_{34}/Q_{43}<1.50$. As may be seen in Tables II.7-II.9, the ratios of the measured cross sections agree with this prediction within a smaller margin than might be expected on the basis of the error assigned to the individual cross sections, indicating a good internal consistency of the results and good accuracy of the relative if not absolute values of the cross sections.

III. LASER-INDUCED FLUORESCENCE SPECTROSCOPY OF Hg_2 MOLECULES

1. Theory

a) Vibrational structure of an Hg_2 band

The internuclear potential V(r) in a diatomic molecule may be represented by a slightly perturbed harmonic oscillator:

$$V(r) = (1/2)\mu(2\pi\omega_e)^2(r-r_e)^2 + \alpha(r-r_e)^3 + \beta(r-r_e)^4, \quad (III.1)$$

where μ is the reduced molecular mass, ω_e is the fundamental vibrational frequency of the harmonic part of the potential, α and β are the coefficients of the Taylor expansion of the potential function at the point of its minimum, r_e denotes the equilibrium internuclear-separation at the potential minimum and r the variable internuclear distance. Equation (III.1) represents an approximate form of the potential (Herzberg 1950) and the approximation, at least for the bottom part of the well, is very good. The model leads to a characteristic configuration of the term-values (energies of the vibrational substates of an electronic energy state):

$$G(v) = \omega_e(v+1/2) - \omega_e x_e(v+1/2)^2 + \ldots, \quad (III.2)$$

where G(v) is the energy of the v-th vibrational level, $\omega_e x_e$ is the anharmonicity and v=0,1,2... denotes the vibrational quantum number.

In a transition between two bound electronic states the relative intensities of various vibrational components can be derived with the aid of the Franck-Condon factors which are proportional to the squares of the respective transition moments (Herzberg 1950):

$$\bar{R}_e^{\,2}\left(\int \psi'_v \psi''_v dr\right)^2, \qquad \text{(III.3)}$$

where $\bar{R}_e$ is the average electronic transition moment over the range of accesible internuclear distances and ψ'_v, ψ''_v are the wave functions of the vibrational levels in the upper and lower electronic states, respectively.

The physical sense of expression (III.3) is commonly known as the Franck-Condon principle which states, that the most probable transitions are those, during which the instantaneous positions of the constituent nuclei and their momenta remain unchanged, while transitions involving changes in nuclear positions or momenta are improbable.

The selection rules for electric dipole transitions are (Herzberg 1950): (g)erade ↔ (u)ngerade, g ↮ g, u ↮ u, + ↔ +, − ↔ − and + ↮ − assuming Hund's case (c) for the coupling of angular momentum in the molecule.

The presence of vibrational substates within an electronic state gives rise to a vibrational structure of molecular bands, observed both in absorption and in fluorescence. An analysis of such an electronic band structure can yield the shape and the location of the molecular potential well. The application of Eq. (III.2) to both upper and lower electronic states involved in a radiative transition yields an expression for the frequencies of vibrational components in an absorption or emission band:

$$\nu_0 = \nu_e + \omega'_e(v'+1/2) - \omega'_e x'_e(v'+1/2)^2 + \ldots$$
$$- [\omega''_e(v''+1/2) - \omega''_e x''_e(v''+1/2)^2 + \ldots], \qquad \text{(III.4)}$$

where ν_e is the frequency corresponding to the electronic transition only (neglecting the vibrational structure) and other symbols are identical with those in Eq. (III.2), referring to the upper state when single-primed and to the lower state when double-primed. Equation (III.4) does not take into account the existence of rotational structure, but can be generalized as follows to include the effects due to rotation:

$$\nu = \nu_0 + B_v J'(J'+1) - D_v J'^2(J'+1)^2 + \ldots$$
$$- [B_v J''(J''+1) - D_v J''^2(J''+1)^2 + \ldots], \qquad \text{(III.5)}$$

where ν_0 is the vibrational frequency, neglecting rotational transitions; J denotes the rotational quantum number and $B_e = h/(8\pi^2 c \mu r_e^2)$ is the rotational constant for a rigid rotator; $B_v = B_e - \alpha_e(v+1/2)$ is the rotational constant corrected for the vibrational distortion of the molecule, where α_e is the correcting factor; D_v is the constant compensating for centrifugal distortion; c is the speed of light and h is the Planck constant. The rotational transitions with $\Delta J=0,\pm1$ ($J'=0 \nleftrightarrow J''=0$) give rise to a large number of spectral components. The mercury molecule has a large mass and moment of inertia, and therefore the rotational spacing near each band-head is smaller by 3-4 orders of magnitude than the vibrational spacing. Additional complications arise from the presence of 21 Hg_2 isotopes into which the 6 abundant Hg isotopes of different nuclear masses can combine; this causes the smearing-out of the rotational structure which becomes quasi-continuous.

Under conditions of thermal equilibrium, the rotational distribution within a vibrational state is given by the Boltzmann law together with the statistical weight factor (Herzberg 1950):

$$N_J \sim (2J+1)\exp[-BJ(J+1)hc/kT], \qquad \text{(III.6)}$$

where N_J is the population of the rotational state with quantum number J. The presence of rotational distributions in all the vibrational states and the variation of rotational constants causes additional loss of definition in the observed spectrum. In order to resolve the rotational structure, very high-resolution spectroscopic methods (preferably Doppler-free) would have to be used, as well as a single Hg isotope.

When a progression of vibrational components in an electronic band has been measured and identified (e.g. frequencies corresponding to transitions $v''\rightarrow v'=$ $0\rightarrow0$, $0\rightarrow1$, $0\rightarrow2$ etc.), then Eq. (III.4) may be used to calculate the energy difference between the two electronic states (more precisely between the v"=0 and v'=0 levels) as well as the zero-point energy and the fundamental vibrational frequency (ω_e') for the upper state. Since the anharmonicity ($\omega_e'x_e'$) is a function of both the α and β coefficients (Herzberg 1950), an analysis of the band structure up to the second order in Eq. (III.4) (which yields ω_e' and $\omega_e'x_e'$) is not sufficient to calculate α and β. Nevertheless, the anharmonicity does provide information about the vibrational spacing as a function of v'. An analysis of a progression (in emission or absorption), consisting of vibrational components due to transitions between a single v' level and a series of v" levels, (e.g. v"↔v'= 0↔0, 1↔0, 2↔0 etc.) leads to the vibrational parameters ω_e'' and $\omega_e''x_e''$ for the lower state. An analysis of a band structure with an accuracy higher than second-order in Eq. (III.4) is, however, seldom possible using methods of conventional spectroscopy because the unresolved rotational structure tends to broaden the spectral lines and makes accurate frequency measurements very difficult.

b) Population of the $G0_u^+$ state

Two different methods may be used to populate the $G0_u^+$ state. Ehrlich and Osgood (1978) effected a direct photoassociation from the ground state using UV excimer laser radiation, while Drullinger et al. (1977) employed a two-stage excitation process in which the first stage produced a high population of the metastable $A0_g^+$ state and the second step involved the subsequent absorption of visible laser light and resulted in the creation of $G0_u^+$ molecules.

Even though the first method is more efficient, it appears less convenient for various reasons. Excimer lasers are not very selective because of their broad-band output (in Ehrlich and Osgood's experiment the band-width was 150 cm^{-1}). Secondly, the laser radiation cannot be tuned, resulting in a limited range of available wavelengths, which, however, may be somewhat enlarged by Raman shifting (Loree et al. 1977). Finally, the excimer laser operates near the edge of the vacuum-ultraviolet spectral region, which requires VUV techniques.

The stepwise excitation method which leads to a relatively high population of the metastable $A0_g^+$ state, has the advantage that this state can then be probed using tunable and efficient dye lasers generating light in the easily accesible visible region. The success of the method hinges on the ability to achieve a large population of the 'reservoir' $A0_g^+$ state.

Because of the selection rules, the direct excitation of an atom-pair from the $X0_g^+$ state to the $A0_g^+$ state is forbidden and the population of the $A0_g^+$ state was accomplished indirectly by a mechanism described by Stock et al. (1977). The presence of (transient) ground-state atom-pairs in the mercury vapour gives rise to an absorption continuum ranging from 3350 Å to 2537 Å (Hg intercombination line), corresponding to the creation of $D1_u$ molecules. Part of the molecules excited to this state decay back to the ground state but, because of the relatively long life of the $D1_u$ state, estimated to be 1.4 μs by Mies et al. (1978), this does not result in a major loss of population, most of which decays through two main channels.

(i) the molecules excited close to the $D1_u$ dissociation limit (6^3P_1 atomic state) undergo collisional mixing with the weakly bound neighboring CO_u^- state (correlated with the atomic 6^3P_0 state) located between the $B1_g$ and $D1_u$ states and not marked in Fig. I.1. As the result of the mixing which takes place near the inner turning point of the repulsive part of the $D1_u$ potential energy curve, the CO_u^- molecules dissociate into pairs of (6^1S_0) and (6^3P_0) atoms. The process can be represented by:

$$2Hg(6^1S_0) + h\nu \longrightarrow Hg_2(D1_u)^* \longrightarrow Hg(6^1S_0) + Hg(6^3P_0), \quad (III.7)$$

where $Hg_2(D1_u)^*$ represents a vibrationally excited $D1_u$ molecule.

(ii) the molecules excited to lower vibrational levels of the $D1_u$ state, located at more than kT below the 6^3P_1 atomic state, undergo collisional thermalization to an equilibrium population distribution among close-lying molecular states (AO_g^-, AO_g^+, $B1_g$, CO_u^-, $D1_u$), as described by:

$$2Hg(6^1S_0) + h\nu \longrightarrow Hg_2(D1_u)^* \longrightarrow (Hg_2)^*, \qquad \text{(III.8)}$$

where $(Hg_2)^*$ is a molecule in any of the above states.

The 6^3P_0 metastable atoms, produced according to Eq. (III.7) also contribute to the creation of an equilibrium population of Hg_2 molecules in various states, according to the equation:

$$Hg(6^3P_0) + 2Hg(6^1S_0) \longrightarrow (Hg_2)^* + Hg(6^1S_0). \qquad \text{(III.9)}$$

In the present case the second excitation channel predominated, as the 2660 Å radiation excited vibrational levels of the $D1_u$ state located much further than kT below the dissociation limit. The $A0_g^-$ and $A0_g^+$ states which are separated by only 20 cm^{-1}, are the lowest bound excited states and, accordingly, one would expect them to become highly populated. While the 0_g^- state cannot participate in the transition to the $G0_u^+$ state, the 0_g^+ state is a metastable state with an effective lifetime of many μs (depending on the ambient Hg density) (Callear and Lai 1979), which acts as an intermediate 'energy reservoir' for transitions to higher excited states (and, in particular, to the $G0_u^+$ state).

c) Band-structure produced by bound-free transitions; Condon internal diffraction

A fluorescence band, originating from a transition between a vibrational level of a bound electronic state and a lower, repulsive electronic state, has a specific profile consisting of a series of 'Condon internal diffraction components' (Condon 1928). Such bands have shapes which qualitatively resemble the probability density distribution of the upper state vibrational wave function. This is illustrated in Fig. III.1 which shows the approximate shapes of the upper and lower potential curves. A molecule, excited to the v-th vibrational level of the $G0_u^+$ electronic state, decays radiatively to the $X0_g^+$ repulsive ground state, where it immediately dissociates.

As originally formulated, the Franck-Condon principle (Franck 1925) requires that the instantaneous positions and momenta of the nuclei must remain unchanged during the transition. Accordingly, the transition is most probable when the relative positions of the nuclei correspond to the antinodes of the upper state vibrational wave function. In addition, the principle of conservation of momentum requires that the kinetic energy of the relative motion of the nuclei must not change during the transition and, consequently, the kinetic energy and the potential energy (including the energy of the photon) are conserved separately (Mulliken 1971). The actual photon energy will therefore be equal to the energy separation between the upper vibrational level and the dotted curve in Fig. III.1 (Ehrlich and Osgood 1979), rather than the potential curve of the ground state, as the balance of the energy appears in the form of the kinetic energy of the two free

Figure III.1. The formation of a Condon internal diffraction pattern in the fluorescence band due to a bound-free transition between a $G0_u^+$ vibrational state and the $X0_g^+$ ground state. The dotted curve represents the excess of kinetic energy which is conserved in the transition. The Condon fluctuations are projected on the E axis.

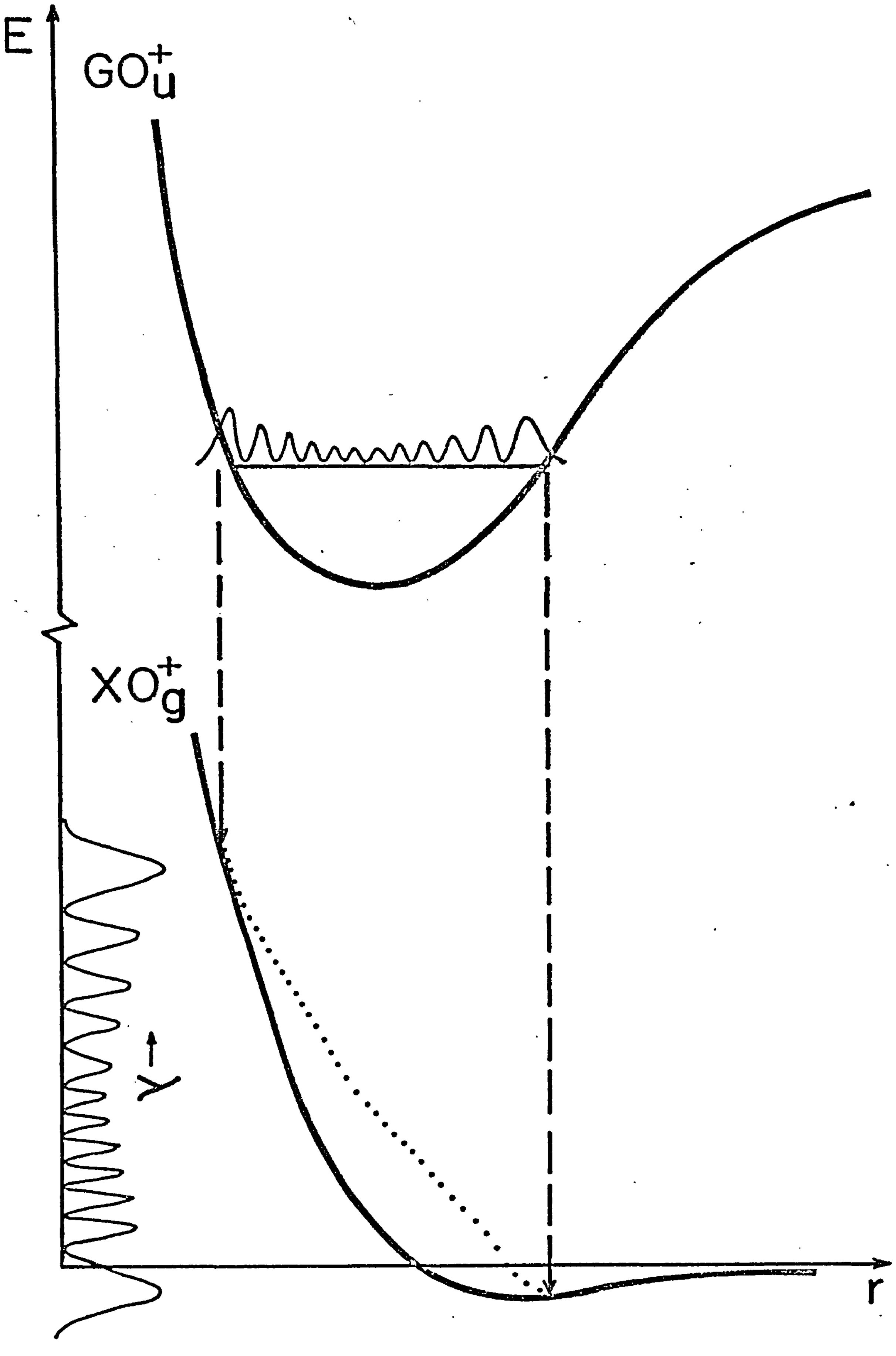
E
GO_u^+
XO_g^+
γ
r

ground-state Hg atoms into which the molecule dissociates.

Because the energy of the emitted photon depends on the instantaneous distance between the nuclei during the transition, the shape of the wave function - or, strictly speaking, of the probability density distribution - will be mapped onto the photon energy scale. This is easily understood when looking at Fig. III.1; the closer together the nuclei are, the higher the radiative transition terminates on the dotted curve. The long-wavelength wing of the spectrum is therefore produced by molecules at short internuclear distance (at the inner classical turning point), while the short-wavelength wing is due to molecules close to the outer classical turning point at the time of the transition. Because of the curvature of the ground-state potential, the mapping is nonlinear and therefore the spacing between the consecutive maxima in the observed fluorescence spectrum will be coarser at its 'red' wing and finer towards its 'blue' wing.

A more rigorous quantum mechanical treatment of bound-free transitions shows that the oscillatory shapes of the fluorescence continua result from the interference of the bound upper-state nuclear (vibrational) wave function with those of ground-state continuum (hence the term 'Condon internal diffraction'). The Franck-Condon integral may be written in the form: $\int \Psi_u(r)\Psi_g(E_K,r)dr$. The essential point of the argument (Mulliken 1971) is that, while Ψ_u is the wave function of the bound upper state, Ψ_g is representative of the continuum of wave functions of the unbound ground state. Ψ_g is therefore a function of two arguments: internuclear separation r, and kinetic energy E_K which is not quantized. Accordingly, the integral, when evaluated, is also a function of kinetic energy and has significant non-zero values when the two following conditions are fulfilled:

(i) the (local) de Broglie wavelengths for both wave functions are equal,

$$\lambda_g = \lambda_u = \lambda = h/(2\mu E_K)^{1/2}, \qquad \text{(III.10)}$$

indicating the conservation of kinetic energy of the nuclei in a transition;

(ii) the phases of both wave functions match (or are shifted by ±π w.r.t. each other) in the local region of r, where $\lambda_g=\lambda_u$.

Since Ψ_u is fixed, $\left|\int \Psi_u \Psi_g dr\right|$ will have maxima for values of E_K which fulfil conditions (i) and (ii). If one of the $\Psi_g(r,E_K)$ functions is varied continuously with respect to the parameter E_K, the relative phase of Ψ_g with respect to Ψ_u will be shifted and the value of the integral will diminish to zero (when the relative phase shift is $\pm\pi/2$), after which $\left|\int \Psi_u \Psi_g dr\right|$ will again reach a local maximum.

E_K can be expressed in terms of the frequency of the photon emitted during the transition:

$$E_K = U_u(r^*) - U_u(r) = U_u(r^*) - U_g(r) - h\nu, \qquad \text{(III.11)}$$

where $U_u(r)$ and $U_g(r)$ are the potential functions of the upper and lower states, respectively, r^* corresponds to the classical turning points of a particular upper-state vibrational wave function and r denotes the small region where $\lambda_u=\lambda_g$ (for a given E_K). The resulting variation in the value $\left|\int\Psi_u\Psi_g dr\right|$ causes fluctuations in the fluorescence intensity across the emitted band, since the transition probability is determined by the squares of the Franck-Condon integrals and, accordingly, the band profile will qualitatively follow the form of $(\Psi_u)^2$.

This model, while explaining reasonably well the qualitative aspects of the spectrum, represents a certain idealization of the real physical situation. Among other things, the presence of rotational effects is ignored; these, when added to the model, would shift both upper and lower potential curves upwards by similar amounts and also reduce the contrast of the fluctuations. This point has been noted by Ehrlich and Osgood (1978), who recorded a Condon diffraction pattern in the fluorescent band which they interpreted as due to the transitions from the v'=57 level of the GO_u^+ state to the XO_g^+ ground state and in which the diffraction components tended to merge into an unresolved continuum towards the short-wavelength end of the band.

Using a semiclassical formalism developed by Tellinghuisen (1975), Ehrlich and Osgood (1978) attempted to obtain an analytical expression for the spacing between the fluorescence intensity maxima in the band as a function of the shapes of the potential curves. Although they produced an approximate expression for the long-wavelength side of the band, the mathematical complexity of the problem would require numerical calculations for a general solution. Furthermore, as shown by Mulliken (1971) and Tellinghuisen (1975), the observed positions and shapes of the fluorescence maxima are slightly distorted by the factor $F(\nu)$ which includes the ν^3-dependence of the emission intensity. A further distortion can be introduced by non-uniformities in the spectral response of the detector.

2. Description of the Apparatus

a) General disposition

The arrangement of the apparatus is shown schematically in Fig. III.2. The 'pump & probe' method was used to excite the $G0_u^+$ state of Hg_2. The fourth harmonic of a Nd:YAG laser was used to produce ('pump') a high population of excited metastable Hg_2 molecules in a fluorescence cell containing Hg vapour. After an appropriate delay, the excited vapour was probed with light pulses originating from a N_2 laser-pumped dye laser. The resulting fluorescence, which was monitored at right-angles to the collinear laser beams, was resolved with a

Figure III.2. Schematic diagram of the apparatus. Dye laser components: O–oscillator, A–amplifier: M–monochromator, PM–photomultiplier, A–D–transient digitizer, D–photodiode, PB–Pellin–Broca prism, X2–frequency doubler.

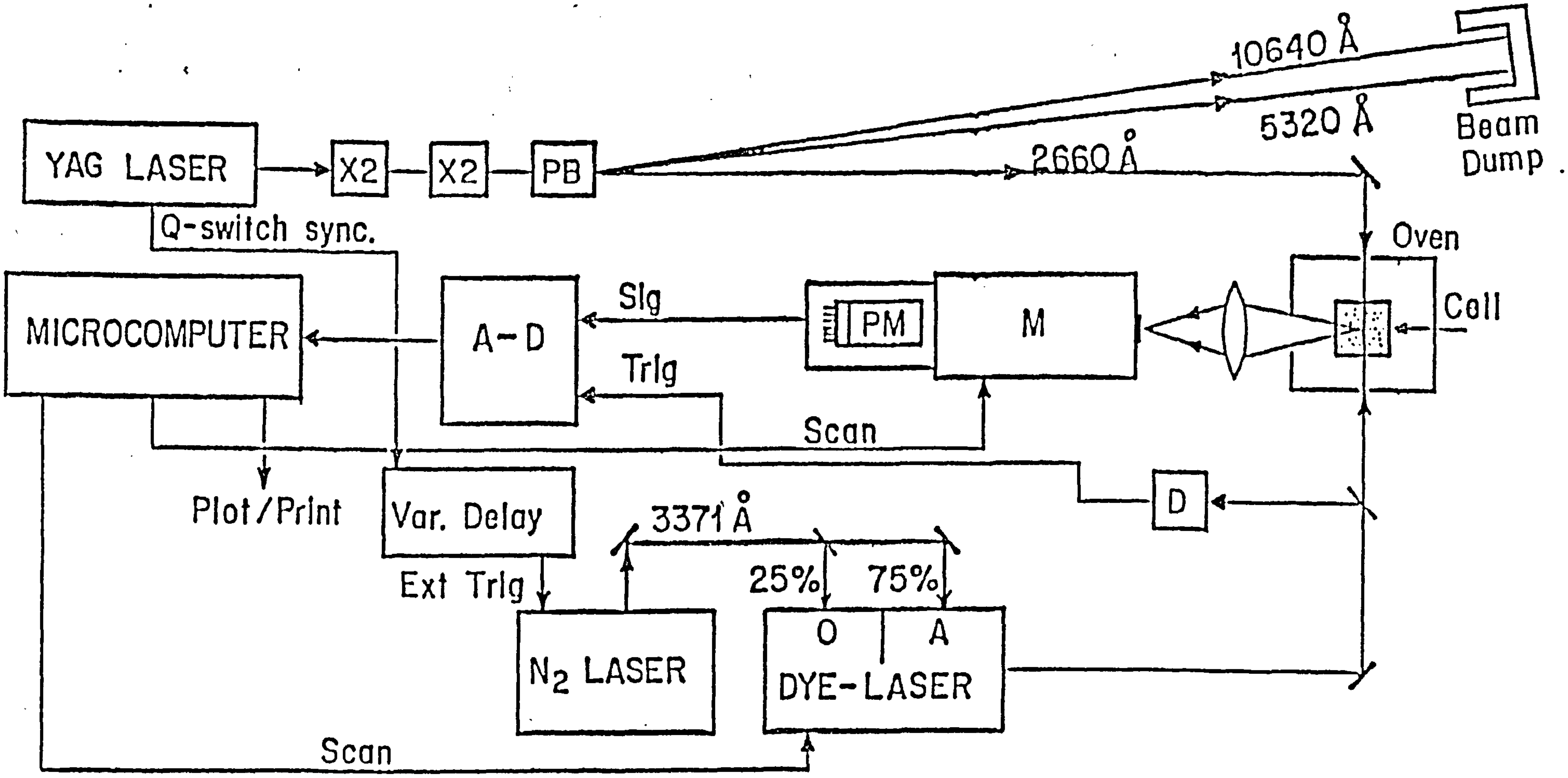
YAG LASER
X2
X2
PB
10640 Å
5320 Å
2660 Å
Beam Dump.
Q-switch sync.
Oven
Cell
MICROCOMPUTER
A-D
Sig
Trig
PM
M
Scan
D
Plot/Print
Var. Delay
3371 Å
25%
75%
Ext Trig
O
A
N_2 LASER
DYE-LASER
Scan

monochromator and detected with a photomultiplier. The probe dye laser and the monochromator could be scanned across the desired wavelength range by means of computer-controlled stepper motors. The output signals from the photomultiplier were recorded with a transient digitizer and the spectra were accumulated in a Commodore Pet 2001 microcomputer.

b) The pump laser

The 2660 Å pumping light beam was generated as the fourth harmonic of a Quanta-Ray DCR-1A Nd:YAG laser which had two stages, an oscillator and an amplifier. It yielded 5-10 ns-wide pulses with the maximal repetition rate of 22 Hz. The fundamental laser output at 10640 Å was emitted in an unstable convex-concave optical resonator equipped with an electro-optical Q-switch (Pockels cell). The laser was always run in the "Q-switched" regime in order to produce short pulses of high peak-power which was required for the efficient generation of higher harmonics. The production of the fourth harmonic was a two-step process. The second harmonic at 5320 Å was first produced using a KD^*P (Potassium Dideuterium Phosphate) frequency-doubling crystal. The crystal was "angle-tuned" for maximal yield. The green 5320 Å output was subsequently passed through another KD^*P crystal, in which the fourth harmonic (2660 Å) was generated. The three output wavelengths, which were collinear, had to be spatially separated. This was accomplished using a Suprasil quartz Pellin-Broca prism. The infrared and second harmonic green output beams were dissipated in a dump-box. The UV beam was conveyed by means of high-power dielectrically coated mirrors.

The diameter of the resulting ultraviolet beam was 6.3 mm; however, before directing the beam into the fluorescence cell, its diameter was reduced to 2-3 mm by means of two lenses arranged as a Galilean telescope. This was done in order to increase the pumping efficiency and to facilitate imaging of the small excited volume on the monochromator slit. The UV beam output energy per pulse was of the order of 15-25 mJ. In most cases sufficient energy was obtained by running the oscillator stage only and omitting the amplifier stage. The transverse uniformity of the beam was less than perfect because of diffraction effects due to irregularities inside the resonator cavity. However, with the beam narrowed to a diameter of about 2-3 mm this did not seem to cause any noticeable difficulties in the excitation process.

c) The probe laser

The probing light beam was generated using an N_2 laser-pumped 2-stage dye laser which was built in-house and closely resembled the laser used in the experiments described in Chapter II. A transverse discharge in the 1 m-long resonator tube, through which pure N_2 gas was forced at a pressure of about 70 torr, provided a pulsed lasing action in a cavity formed by a flat total reflector and a flat quartz glass plate which acted as the output window. The pulse length was found to be of the order of 5 ns. As the N_2 laser was triggered externally by the Q-switched pulse of the YAG laser, its repetition rate was governed by the YAG rate which was usually set at about 15 Hz.

The N_2 laser output was divided into two parts. The first, constituting approximately 25% of the total, was used to pump the oscillator stage of the dye laser while the remaining 75% were used to excite the amplifier stage. Both stages were side-pumped and aspheric quartz lenses were used to focus the N_2 laser output into the magnetically stirred dye-cells. The dye laser oscillator cavity included a quad-prism unidirectional beam expander (Niefer 1983) and was tuned by means of a diffraction grating. The process of tuning the dye laser was automated by using a microcomputer-controlled stepper motor to rotate the grating. The finest step of the motor was found to correspond to a spectral frequency increment of 0.2-0.5 cm^{-1}, depending on the order of diffraction used for oscillator feedback. The spectral band-width of the dye laser output, as measured with a Fabry-Perot etalon, was of the order of 0.2 cm^{-1}, depending somewhat on the focussing of the pumping N_2 laser light inside the oscillator dye-cell (stronger focussing resulted in larger gain due to stimulated emission and caused broadening of the laser line). The output radiation was passed through an aperture 3 mm in diameter, which was placed close to the dye laser, to reject unwanted superradiance which otherwise might find its way into the fluorescence cell and produce spurious signals (e.g. by scattering off the cell walls). The direction of the dye laser beam was found to be independent of the wavelength and, in spite of the considerable distance between the laser and the cell (3 m), no deviation of the beam was observed during the wavelength scans.

The N_2 laser was triggered by a delayed electric pulse available from a Q-switch-synchronized outlet of the YAG laser. A Berkeley Nucleonics 7010 delay generator controlled the delay between the YAG and N_2 laser pulses, which could be varied from about 700 ns (the lower limit of the pulse-handling and triggering electronics) to several ms. The strength of the observed signal was not particularly sensitive to the delay time in the range 1-10 μs and the delay time was usually set at a value ranging from 1.5 to 5 μs.

Several laser dyes were used in the experiments, producing light at wavelengths from 5000 Å to 6500 Å. The dyes are listed in Table III.1. Since the relative efficiency of the various dyes was much lower at the wings of the output bands than at the centres, it was important to have the bands overlap in order to produce optimal fluorescent intensities.

TABLE III.1 Laser dyes used in the experiment

wavelength range (Å)	dye	molar concentration (in ethanol)
4950-5250	Coumarin 500	5.4×10^{-3}
5200-5500	Coumarin 540A	1×10^{-2}
5450-5750	Cou 540A/Rh 6G	$5\times10^{-3}/3\times10^{-3}$
5700-6000	Rhodamine 6G	5×10^{-3}
5950-6290	Rhodamine 610	5×10^{-3}
6150-6400	Rh 610/Rh 640	$2.5\times10^{-3}/3\times10^{-3}$
6200-6550	Rhodamine 640	5.7×10^{-3}

d) The fluorescence cell and the oven

The fluorescence cell was cylindrical in shape, 7 cm long and 4 cm in diameter, and was made of Suprasil quartz. It had a sidearm, approximately 15 cm long and 1.5 cm in diameter, which served as a reservoir for the liquid mercury (triple-distilled natural mercury was supplied by Engelhard Industries).

Before being mounted in the oven, the cell was subjected to thorough cleaning and outgassing. It was first washed with a solution of HF and, after careful rinsing with distilled water, was connected to the vacuum system. A four-stage mercury distillation column was connected to the same system, which was evacuated and baked out for approximately 2 days. When the vacuum stabilized at about 1×10^{-8} torr, a sealed ampoule containing mercury was broken using a magnetic breaker and the process of distillation was accomplished under high vacuum. The liquid mercury was introduced into the cell which was then sealed off.

The vacuum system consisted of an Edwards ED 100 rotary pump and a 4" diffusion pump fitted with a butterfly valve and a liquid N_2-filled cold trap. It also included, as a final stage, a titanium getter-pump and another cold-trap. The vacuum system and the cell were baked out to drive-off contaminants adsorbed on surfaces. The glass system was baked using heating tapes and an electrically heated oven was used to bake the cell at temperatures reaching 900 K.

The sealed cell, with the sidearm extending downwards, was mounted in a two-compartment oven. The main compartment, containing the body of the cell, was a cubical box with double walls. The outer wall was made of copper-clad aluminum and the inner wall was made of stainless steel and lined with asbestos. The side walls of the oven were fitted with centrally located demountable quartz windows about 4 cm in diameter, fastened by aluminum rings. Two of the windows provided access for the laser beams, another was the exit window, through which the fluorescent light reached the spectrometer, and the fourth window permitted visual inspection of the fluorescence and facilitated adjustments of laser beam-handling optics for maximal beam overlap inside the cell. The space between the inner and the outer oven walls was filled with soft mica chips. To make the construction more rigid, several ceramic spacers were placed between the walls. Coils of resistance wire of combined resistance about 70Ω were mounted on insulating asbestos pads on the walls of the inner oven cavity and served as electrical heating elements.

The oven compartment containing the cell side-arm extended below the main oven. It was smaller, cylindrical in shape and had its own heating element whose total resistance was about 18Ω.

The two heaters were connected to two Variac autotransformers which controlled the currents and permitted the independent adjustment of the temperatures of the side-arm and of the main body of the cell. Two chromel-alumel thermocouples were fastened to a ceramic collar surrounding the liquid mercury reservoir and two others were located inside the main oven cavity, at about 1 cm from the cell. The thermocouples were connected to a digital voltmeter and were used to monitor the temperature distribution in the oven.

The outer surface of the oven was cooled with tap-water passing through copper tubing (6.3 mm in diameter) soldered to the oven wall. This was done to keep the temperature of the oven surface at about 15°C while the interior temperature frequently exceeded 400°C during the experimental runs.

e) The spectrometer and data-acquisition system.

The fluorescence light which passed through the cylindrically shaped side-wall of the cell and the quartz window in the oven wall, was focused on the entrance slit of the monochromator by a spherical quartz lens of 20 cm focal length. The monochromator was manufactured by Jobin-Yvon and utilized a 1200 l/mm concave holographic grating which provided a relatively high spectral response (30-35%) in the ultraviolet. The focal length of the monochromator was about 20 cm, and its effective speed was f/4.2. With 1/8 mm entrance and exit slits the instrument had a resolution of 3-4 Å (62-83 cm^{-1}) at 2200 Å.

The incomplete rejection of the unwanted visible scattered dye laser light created some difficulties, since the scattered light gave rise to a background in the recorded spectrum, which varied slowly with the laser wavelength. Depending on experimental conditions, this background contributed 5-25% of the total signal and could not be completely eliminated.

The monochromator was fitted with an EMI 9816 QB photomultiplier which had an extended S-20 photocathode and a 14-dynode electron multiplier. Its spectral response was very good in the spectral range 2000-2400 Å which encompassed the observed fluorescence, and no additional amplification was necessary. The photomultiplier rise time was 2.2 ns and, although the tube was rated at 3 kV, a potential difference of 1.9 kV (supplied by an Ortec 456 power supply) was sufficient to obtain a satisfactory signal. The photomultiplier was mounted in an EMI thermoelectric cooling unit in order to reduce dark noise. The wavelength drive of the monochromator was fitted with a stepper motor which permitted computer-controlled scanning of the spectrum.

The output signal was recorded with a Biomation 6500 waveform analyzer acting as a transient digitizer. It was triggered by a fast EG&G photodiode which was activated by a small fraction of the dye laser output taken off with the aid of a beam-splitter. In this way the instrument accepted and time-analyzed the incoming fluorescence signal following each exciting laser pulse. 1024 memory channels were available, corresponding to sequential time periods ranging from 2 ns to 1 s/channel. The digitized signals were transferred to a Commodore PET 2001 microcomputer. An appropriate program, written in machine language (Niefer 1985), was used to carry out signal averaging of the incoming data and to control the processes of scanning the monochromator and the dye laser. The computer display screen was programmed to display the important experimental parameters, such as the lower and upper limits of the scanned wavelength region, the actual wavelength setting, the scanning increment, the current magnitude of the incoming signal, as well as a histogram showing the most recent recording of the spectrum produced by the signal-averaging process. After each experimental run the results were printed and plotted on an Epson MX-80 printer.

3. Experimental Procedure

a) General description

The pulsed 2660 Å pumping radiation from the YAG laser was used to create a population of metastable AO_g^+ Hg_2 molecules in the fluorescence cell. After an appropriate delay, a spatially overlapping pulse of visible radiation from the probe laser excited the AO_g^+ molecules to the short-lived GO_u^+ state. An ultraviolet fluorescence band was observed, originating from the radiative decay of the GO_u^+ state to the virtually repulsive XO_g^+ ground state. The spectrum was analyzed with the scanning spectrometer, was time-resolved and registered with the transient digitizer, and was transferred to the microcomputer memory for signal averaging. Two separate types of experiments were carried out. In one procedure the fluorescence was excited with probe radiation of fixed wavelength while the fluorescence band was scanned with the spectrometer. The second procedure involved scans with the probe laser across the AO_g^+ absorption spectrum while the fluorescent emission was registered at a fixed wavelength setting of the spectrometer.

b) Spectrometer scans of the fluorescence spectrum in the 2000-2400 Å region

The pump and probe laser beams were made incident on the Hg vapour and were brought into overlap manually, while their relative positions in the cell were observed visually. The adjustment of the laser beams for maximal overlap was found to be critical and had to be done very carefully to ensure a satisfactory level of fluorescence intensity. The observed signal was also sensitive to the position of the lens which focused the fluorescing region in the vapour on the monochromator slit. The optical adjustments were carried out while monitoring an oscilloscope which displayed the transient digitized signal. The time delay between the two laser pulses was kept within the range 1.5-5 μs. The scanning limits of the spectrum were entered into the microcomputer, as was the scanning wavelength increment, which was rarely smaller than 2 Å.

The following 'Boxcar' averaging procedure was used to measure the amount of fluorescence in each wavelength increment of the scanned spectrum. The time-resolved fluorescent signal due to a single dye laser pulse was integrated by the microcomputer over the time interval of about 40 ns, after which no significant amount of fluorescence was observed. The result of this integration was momentarily displayed on the computer screen in the form of a horizontal bar whose length was proportional to the integrated signal intensity. After having accepted the signal produced by a preset number of laser pulses (usually 20 or 25), the microcomputer would sum the resulting count, store it in its memory and advance the monochromator setting to the subsequent position where this procedure would be repeated. After scanning through the preset limits of the spectrum, the grating drive would return to its initial position, to begin the next scan. An accumulation of several scans produced a considerable improvement of the signal-to-noise ratio in the resulting spectrum which was represented in terms of the relative fluorescence intensities for each of the small segments corresponding to the wavelength scanning increments. The time-evolution of the observed fluorescence was found to be identical (within the time-resolution capability of the transient digitizer) with that of the dye laser pulse, indicating an extremely short lifetime of the $G0_u^+$ state. Consequently, only about 20 initial channels (each corresponding to 2 ns) in the transient digitizer were used, which were found to contain close to 100% of the observed fluorescence.

This procedure was repeated several times for various (fixed) wavelengths of the probe laser and using the narrow (1/8 mm) monochromator slits to obtain the best available resolution of the band structures.

c) Probe laser scans in the 5000 Å - 6500 Å region

The apparatus and experimental procedure were as described previously, though with one important difference.

The spectrometer was set at a fixed wavelength while the probe laser was scanned across the wavelength range of the dye by means of a stepper motor which changed the tuning angle of the diffraction grating in the laser cavity. As before, the scanning process was controlled by the microcomputer which also handled the data. Several dyes listed in Table III.1 were used in the probe laser to cover the wavelength range 5000-6500 Å. The scanning increments which were produced by the stepper motor ranged from 0.2 to 0.5 cm^{-1}, depending on the order of diffraction utilized in the feedback of the dye laser oscillator. However, in most cases, the observed band structure became apparent when scanning the dye laser at about 3 cm^{-1} per step, which corresponded roughly to wavelength increments of 1 Å. The observed resolution of the band structure could not be improved by scanning the laser in finer steps.

Since the laser-induced fluorescence bands, produced in this way, were quite broad, correspondingly wider slits (0.5-1 mm) were used in the monochromator to increase the fluorescent signal, with a UV pass-band filter placed in front of the entrance slit to reduce the scattered laser light.

During such scans the monochromator was usually set at 2200-2250 Å. The profile of the fluorescence spectrum was found to be independent (within experimental error) of the monochromator wavelength setting within limits 2100-2300 Å, though the integrated band intensities differed, depending on the wavelength at which the fluorescence was recorded.

4. Results and Discussion

a) Analysis of the fluorescence bands in the 2000-2400 Å region

Figures III.3-III.4 show representative traces of fluorescence bands, each excited with a particular wavelength of the probe radiation and arising from the decay of a particular v' level. It is apparent that the width of the band and the number of resolved components decrease as the wavelength of the probe radiation is increased. Although the bands exhibit some significant departures from the predictions of the model described in section III-1c, they are amenable, at least in part, to quantitative analysis.

It may be seen that the contrast between the maxima and minima is much lower than the theoretically predicted value of 100% which would be expected in the absence of rotational structure and the isotope effect. In addition, although the diffraction components on the long-wavelength side of each band are fully resolved, they appear to be 'washed out' towards the short-wavelengths, except for the intense final component corresponding to the outer classical turning point of the wave function. These imperfections are partly instrumental and partly physical

Figure III.3. Traces of laser-excited fluorescence bands arising from the decay of selectively populated v', $G0_u^+$ states and showing Condon internal diffraction patterns. A: v'=16-18; B: v'=14±1; C: v'=11 and 13; D: v'=7 or 8. In each case the wavelength of the probe radiation is indicated, the error bars are typical for each signal-averaged trace.

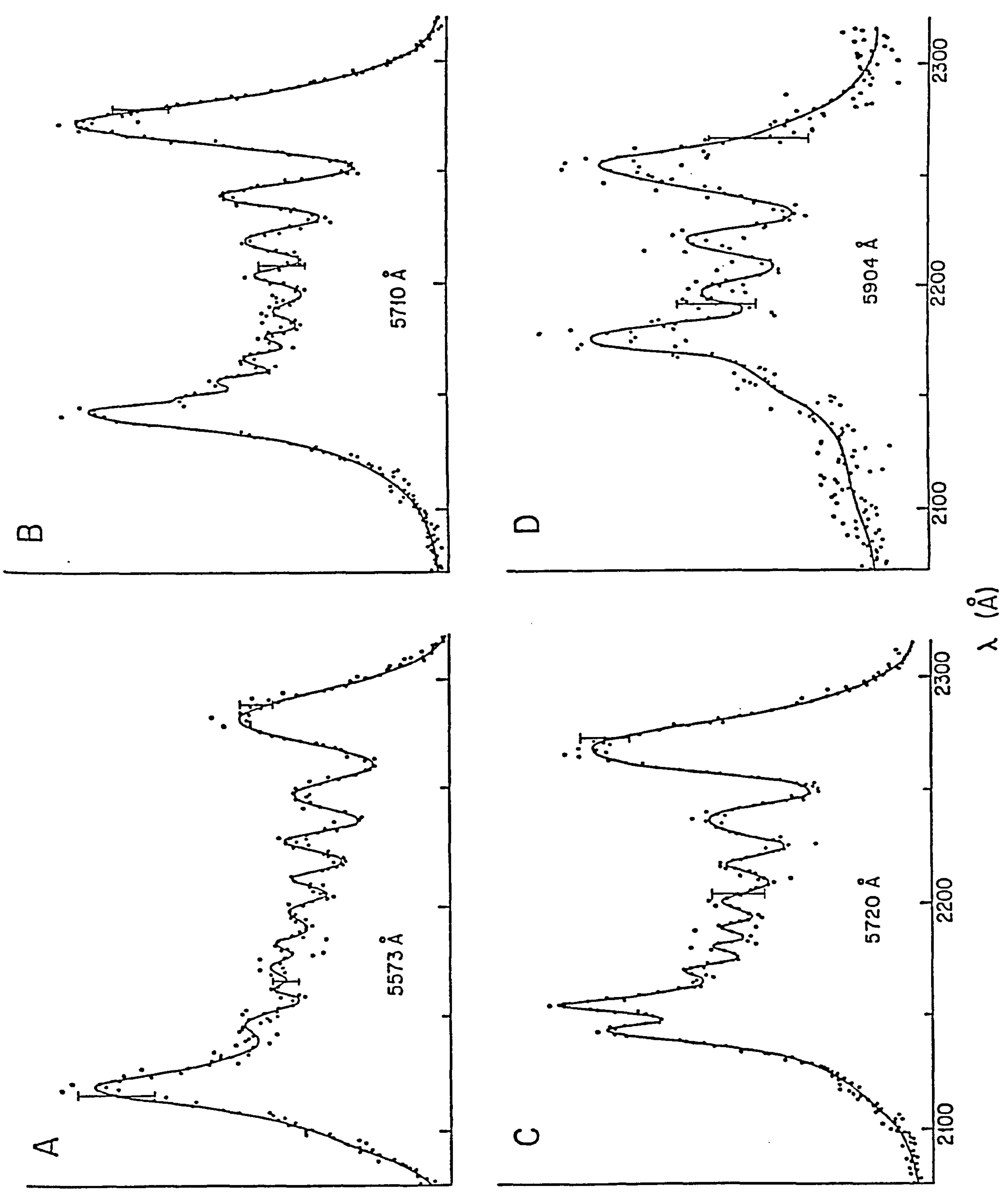
A
5573 Å
B
5710 Å
C
5720 Å
D
5904 Å
2100
2200
2300
2100
2200
2300
λ (Å)

Figure III.4. Traces of laser-excited fluorescence bands arising from the decay of selectively populated v', $G0_u^+$ states and showing Condon internal diffraction patterns. A: v'=0; B: v'=4; C: v'=5; D: v'=0. In each case the wavelength of the probe radiation is indicated, the error bars are typical for each signal-averaged trace. The wavelength scale for A and C is different than for B and D.

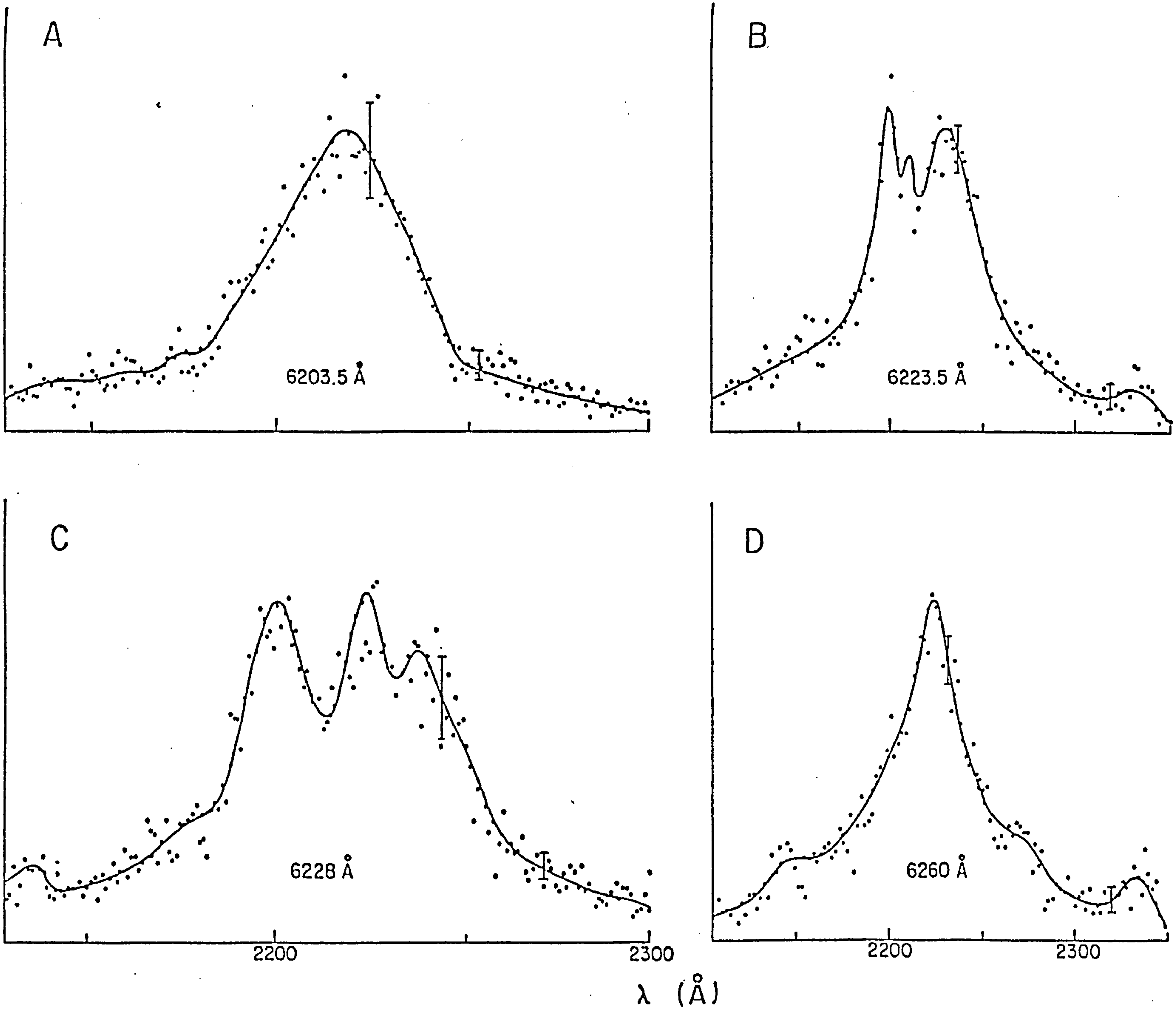
A
6203.5 Å
B
6223.5 Å
C
6228 Å
2200
2300
D
6260 Å
2200
2300
λ (Å)

in origin. The imperfect resolution of the band structure is certainly due in part to the limitations of the monochromator whose resolution (3-4 Å) was lower than the figure of 2 Å quoted by Ehrlich and Osgood (1978) who observed resolved structure in their band somewhat further towards the short wavelengths. The unfavourable signal-to-noise ratio which may be seen in Figs. III.3-III.4 is due to the relatively low population density of the $A0_g^+$ metastable state produced by the pump laser, which in turn limits the population of the $G0_u^+$ state and thus the intensity of the fluorescent band. By comparison, the 'photoassociation' of ground-state atoms employed by Ehrlich and Osgood is a considerably more efficient excitation process which produces a higher band intensity and a better s/n ratio, particularly at higher Hg vapour densities, since the yield depends on the square of the Hg density.

The certain lack of definition and clarity in the band structure also arises from the fact that not all $A0_g^+$ molecules are excited to a single v' level in the $G0_u^+$ state, even when a narrow probe laser band is being used. The $A0_g^+$ molecules have a Boltzmann vibrational distribution and, consequently, the probe radiation can excite numerous v"→v' transitions. Since the energies of many such transitions are nearly equal and, because of broadening caused by rotational structure, pressure, and isotope effect, various v"→v' absorption bands overlap the probe laser band-width.

An important objective of this experiment was to find the wavelength of the probe radiation, corresponding to the $v''=0 \rightarrow v'=0$ transition between the $A0_g^+$ and $G0_u^+$ states, and to determine the wavelength of the UV fluorescence emitted in the decay of the $v'=0$, $G0_u^+$ state to the $X0_g^+$ ground state. The probe wavelengths, used to excite the fluorescence, were chosen to correspond to peaks in the $A0_g^+$ absorption spectrum, which were located as described in section (b). As might be expected, this procedure produced a predominant population of a particular v' state for each exciting wavelength, and the decays of various v' states to the repulsive $X0_g^+$ ground state gave rise to the bands traced in Figs. III.3-III.4. That each band arises from a single v' state is apparent from the form of the Condon diffraction patterns which have two prominent peaks, one at each end, corresponding to the classical turning points of the particular v' wave function. By this token, the band trace shown in Fig. III.3C suggests that two vibrational states must have been excited simultaneously (and to a comparable extent), possibly because of wavelength overlap and favourable Franck-Condon factors. This can be seen especially clearly at the short-wavelength side of the spectrum, where there are two (rather than one) distinct diffraction peaks corresponding to the innermost extrema of two different wave functions. In the 'red' wing this particular feature is not so apparent since the positioning of the peaks at this wing is much less sensitive to the vibrational quantum number of the upper state.

Using probe radiation of sufficiently long wavelength, it should be possible to excite the v'=0 state whose decay would give rise to a fluorescence band consisting of a single and relatively narrow peak corresponding to the shape of the wave function of the v'=0 state. The trace of such a band at λ=2225±2 Å, which was obtained using a probe wavelength of 6203.5±1 Å, is shown in Fig. III.4A. There is good circumstantial evidence that the transition induced by the 6203.5 Å probe radiation is the v"=0→v'=0 transition and that the band is emitted by the v'=0 level of the $G0_u^+$ state decaying to the repulsive $X0_g^+$ ground state. The single-peaked UV fluorescence profile, recorded using this wavelength, constitutes clear proof that the v'=0 state is the emitting state for this band. The fact that the excitation of the band by the probe radiation takes place <u>from the v"=0 state</u> is borne out in Fig. III.5 which shows various v"→v'=0 transitions, among which the v"=0→v'=0 transition must correspond to the shortest wavelength of the exciting radiation. Since no emission was observed from the v'=0 state when using exciting probe radiation of wavelengths shorter than 6203.5 Å, I believe that this wavelength defines the v"=0→v'=0 transition. It should be noted that hypothetical shorter wavelengths can be calculated from the known vibrational spacing of the $A0_g^+$ state (Callear and Lai 1980; Niefer et al. 1983b). Attempts

Figure III.5. PE curves of states participating in the absorption and emission processes, showing the unambiguous location of the $v''=0 \rightarrow v'=0$ transition in absorption. The diagram is not drawn to scale.

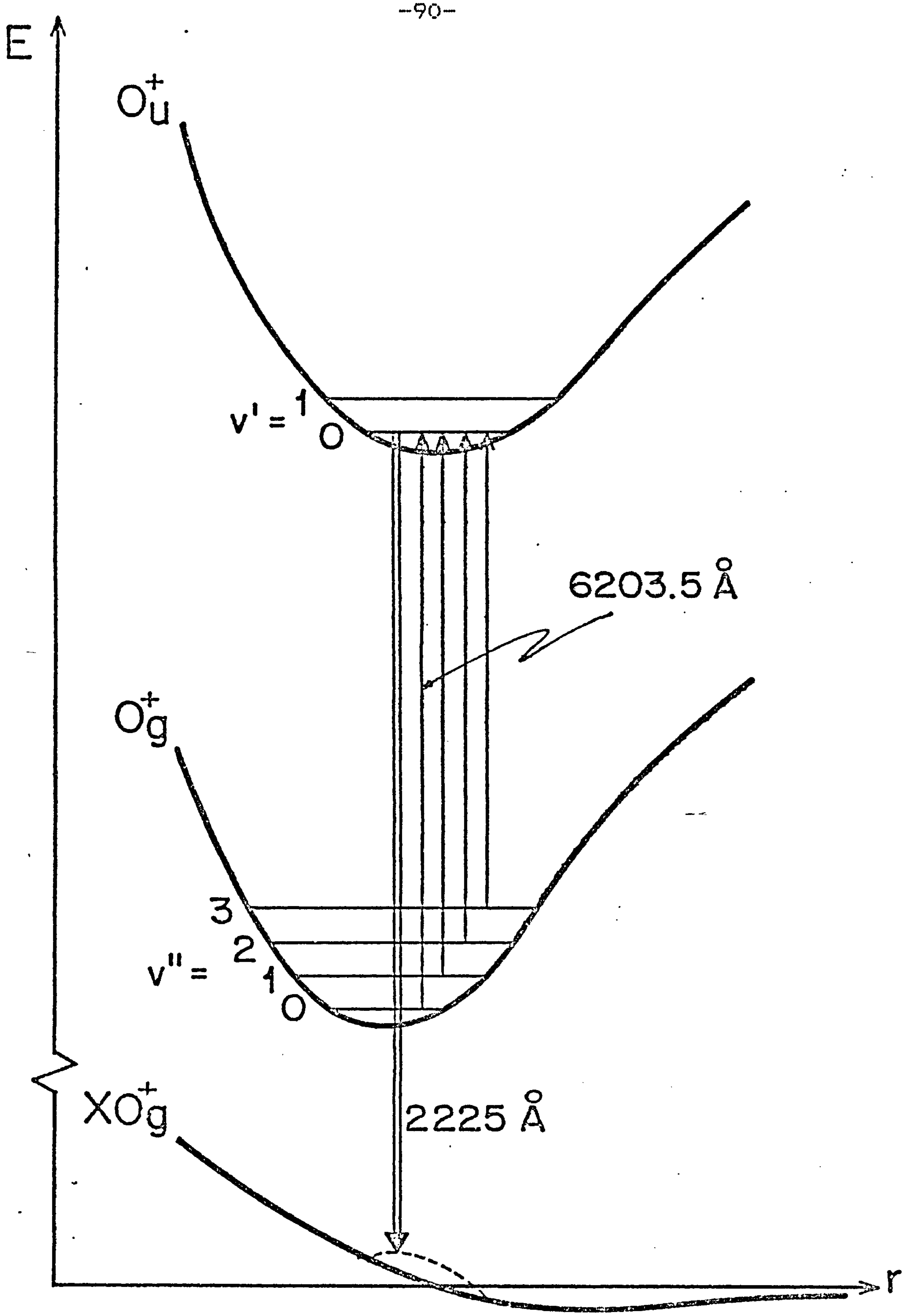
E
O_u^+
v' = 1
0
6203.5 Å
O_g^+
3
2
v'' = 1
0
XO_g^+
2225 Å
r

to probe the vapour with such shorter-wavelength radiation did not, however, produce any detectable population of the v'=0 state. The slight possibility that the 6203.5 Å radiation corresponds to some other (v">0→v'=0) transition in absorption cannot be totally ruled out as the relative strengths of transitions can vary quite dramatically with v" and v' (Condon 1947), and the weakest among them may be difficult to detect. However, the absorption strength of other transitions, with v">0→v'=0, observed in the experiment, was found to vary rather slowly and monotonically with v". This observation implies, that the strengths of two such v">0→v'=0 neighboring spectral components are most unlikely to differ by an order of magnitude, probably because two wave functions belonging to low-lying vibrational levels of two potentials having different r_e values, overlap significantly only in the classically inaccesible regions, where they are not oscillating, and the Franck-Condon integral is sensitive to their overlap (Mies et al. 1978).

The measured wavelength λ=6203.5 Å yields the energy separation of 16115.6±3.0 cm^{-1} or 1.998 eV between the $A0_g^+$ and $G0_u^+$ states. Although this value corresponds to the energy separation between the v"=0 and v'=0 levels of these states, I estimate [using Eq.(III.2) and results presented in section (b)] that the zero-point energy in the lower state exceeds that of the upper state by only about 6-8 cm^{-1} and, consequently, the actual spacing between the minima of the potential wells is 16122.0±5.0 cm^{-1}. Drullinger et al. (1977), using Mosburg and Wilke's (1977) results, assigned the value of 3.59 eV to the minimum of the $A0_g^+$ potential curve and it follows that the $G0_u^+$ potential curve has a minimum at 5.59 eV. The accuracy of this result depends mainly on the accuracy of Drullinger's value for the $A0_g^+$ state. Although Mies et al. (1978) calculated the position of the $G0_u^+$ potential minimum to be about 5.85 eV, the authors concede that their model tends to underestimate the depth of the potential well by roughly 0.5 eV. [They also calculated the $D1_u$ potential minimum to be about 4.55 eV which should be compared with the experimental value of 3.90 eV determined by Smith et al. (1977)].

I believe, that the 2250 Å fluorescence band reported by Hamada (1931) and by Drullinger et al. (1977) corresponds to a superposition of various $v'(G0_u^+)$ decays, such as those represented in Figs. III.3-III.4. Some of these decays involving v'>0 states, would terminate much higher on the repulsive part of the ground-state potential curve, producing fluorescence of longer wavelengths. Besides, both papers reported a fairly broad fluorescence band: the band observed by Drullinger et al. (1977) extended over 200 Å and an even broader band was recorded by Hamada (1931). My value of 2225 Å for the v'=0 component lies well within these limits.

The results of this experiment can be used to derive or verify parameters associated with the molecular states involved in the transitions. Using Baylis' (1977) calculation of the XO_g^+ potential, in conjunction with the value $r_e = 6.1\ a_0$ for the equilibrium internuclear separation in the GO_u^+ state, calculated by Mies et al. (1978), it is possible to estimate the position on the XO_g^+ potential curve, at which the $v' = 0\ (GO_u^+) \rightarrow XO_g^+$ transition terminates. This end-point is located at $1-2 \times 10^{-2}$ eV (81-161 cm^{-1}) above the atomic ground state as shown in Fig. III.6. This value, when combined with the energy of the 2225 Å radiation (44930 cm^{-1} or 5.571 eV), yields the GO_u^+ potential minimum at 5.58-5.59 eV; the potential minimum of the AO_g^+ state may then also be fixed at 3.58-3.59 eV using the measured wavelength 6203.5 Å corresponding to the $v''=0\ (AO_g^+) \rightarrow v'=0\ (GO_u^+)$ transition. These measurements, together with the calculated ground-state potential (Baylis 1977), provide independent confirmation for $r_e\ (GO_u^+)$ calculated by Mies et al. (1978), and for the energy of the AO_g^+ potential minimum reported by Drullinger et al. (1977) to be 3.59 eV. Even though calculations of potential energy curves are subject to errors inherent in the particular model and it is possible that the agreement between the experimental and theoretical absolute values of the various energy levels is coincidental, I believe that the relative energy spacings are reasonably correct and are accurate within the stated limits of error. The various parameters for the XO_g^+, AO_g^+

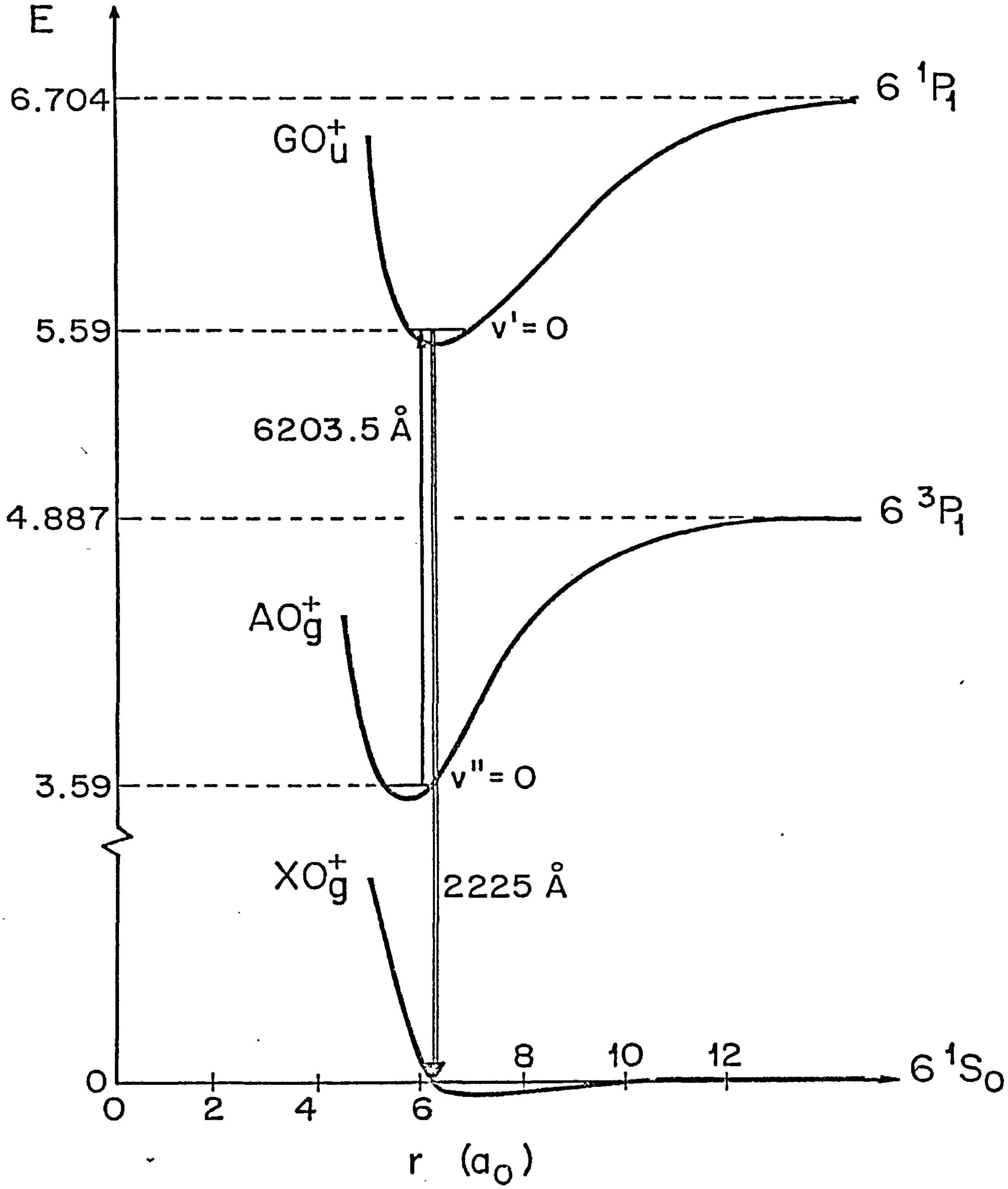
E
6.704
5.59
4.887
3.59
0
GO_u^+
AO_g^+
XO_g^+
$6\,^1P_1$
$6\,^3P_1$
$6\,^1S_0$
v' = 0
v'' = 0
6203.5 Å
2225 Å
0
2
4
6
8
10
12
r (a$_0$)

and GO_u^+ states are collected in Tables III.2 and III.3.

b) The absorption spectrum in the 5000 Å - 6500 Å region, monitored through the emission of UV fluorescence

The UV fluorescent emission observed at a fixed wavelength setting of the spectrometer, when carrying out wavelength scans with the probe laser, represents the vibrational structure of the $AO_g^+ \rightarrow GO_u^+$ absorption band since the $GO_u^+ \rightarrow XO_g^+$ fluorescent decay constitutes the main channel for the deexcitation of the GO_u^+ state; collisional decay (quenching) is not significant because of the extremely short lifetime of the GO_u^+ state (~1 ns).

The aim of these experiments was the determination of the vibrational constants (ω_e' and $\omega_e'x_e'$), and the confirmation of the value found for the $v''=0 \rightarrow v'=0$ transition energy. Several scans with various laser dyes encompassing the spectral range 5000-6500 Å were performed and typical bands resulting from such scans are shown in Figs. III.7-III.9. In each case the band exhibits fairly extensive and often irregular structure, superimposed on a continuous background which usually accounts for up to 60% of the total signal. At least two scans were carried out (on different days) in each spectral region (with each laser dye) to ensure reproducibility of the spectra. The fluorescence appeared to be most intense in the 5500-5750 Å scanning region and gradually faded at longer and shorter wavelengths, a feature which is not immediately apparent

TABLE III.2. Energies and equilibrium internuclear separations for $X0_g^+$, $A0_g^+$ and $G0_u^+$ states of Hg_2

Hg_2 state	equilibrium internuclear separation $r_e(a_0)$	energy at potential minimum (eV)
$X0_g^+$	6.9 ± 0.7[a)]	−0.055 ± 0.011[a)] −0.057[b)]
$A0_g^+$	~ 5.7[c)]	3.59 ± 0.04[b)] ~ 4.19[c)]
$G0_u^+$	~ 6.1[c; d)]	~ 5.85[c)] 5.59 ± 0.04[d)]

[a)] Baylis (1977)

[b)] Drullinger et al. (1977)

[c)] Mies et al. (1978)

[d)] this investigation; the value is subject to errors in the energy of the $A0_g^+$ state

TABLE III.3. Energy gaps between molecular Hg_2 and atomic Hg states

energy states	energy separation (cm^{-1})
$G0_u^+ - A0_g^+$	$16122.0 \pm 5.0^{a)}$ $\sim 13400^{b)}$
$G0_u^+(v'=0) - X0_g^+$	$44930 \pm 40^{a)}$
$G0_u^+ - 6^1S_0$	$45050 \pm 80^{a,c)}$

a) this investigation

b) Mies et al. (1978)

c) Baylis (1977)

Figure III.7. Traces of the fluorescence-monitored $A0_g^+ \longrightarrow G0_u^+$ absorption spectrum. A: 5540–5760 Å region; B: 5700–5995 Å region. The dashed curves indicate relative dye laser output power. No attempt was made to identify the components in the spectrum.

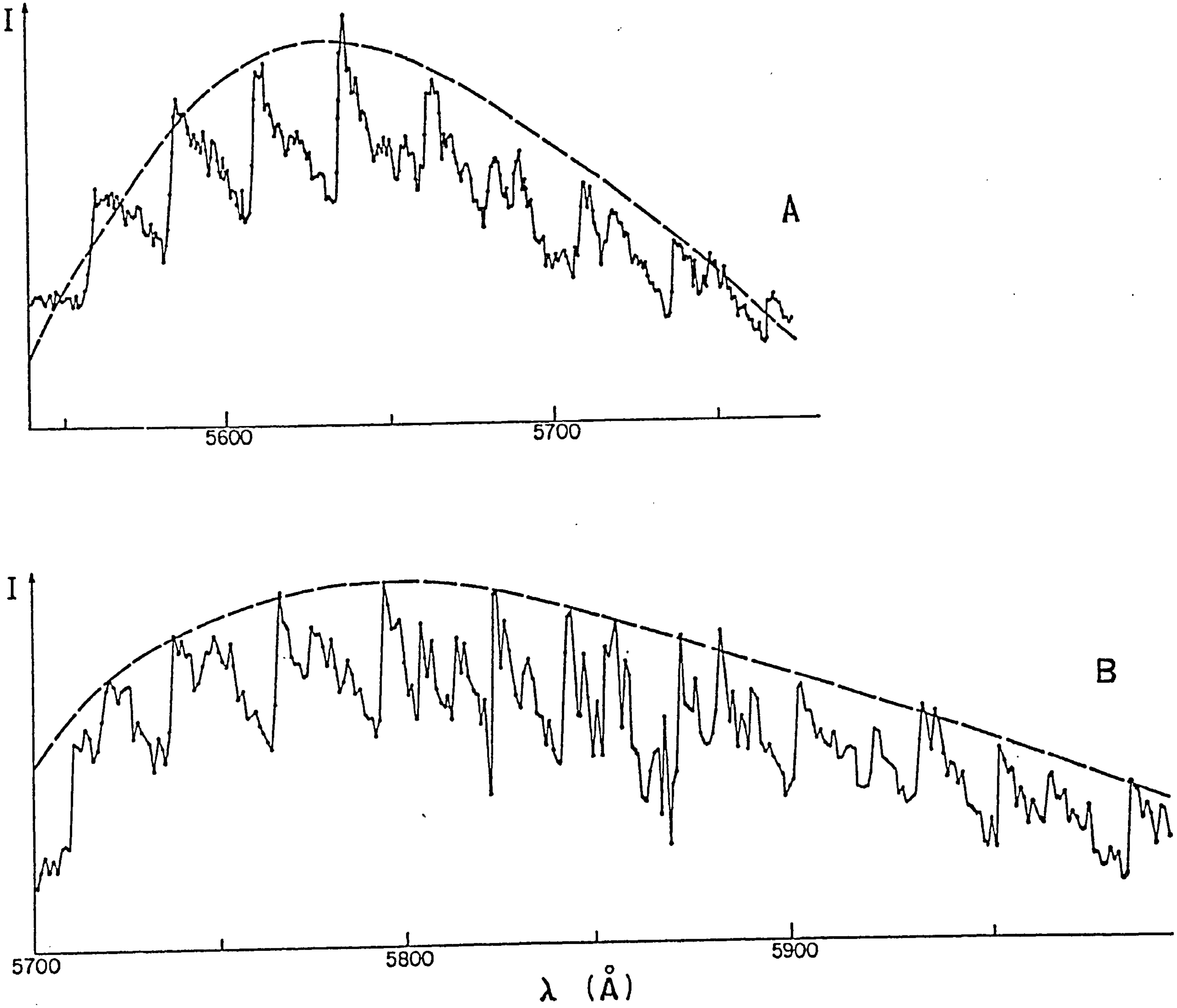
I
A
5600
5700
I
B
5700
5800
5900
λ (Å)

Figure III.8. Traces of the fluorescence-monitored $A0_g^+ \longrightarrow G0_u^+$ absorption spectrum, showing $v'' \longrightarrow v'$ assignments. A: 5980-6260 Å region; B: 6150-6400 Å region. The dashed curves indicate relative dye laser output power.

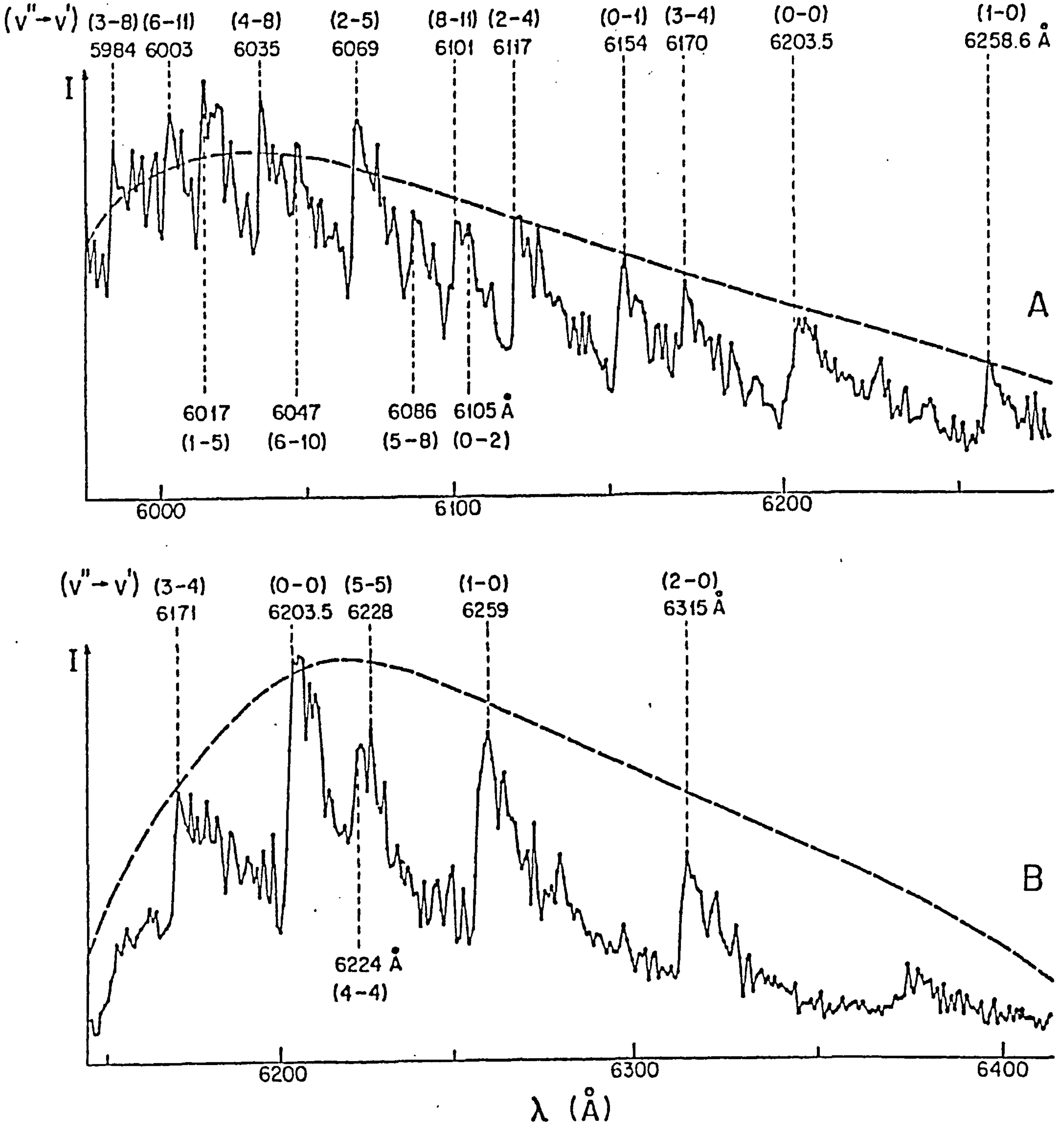
(v''→v') (3-8) (6-11) (4-8) (2-5) (8-11) (2-4) (0-1) (3-4) (0-0) (1-0)
5984 6003 6035 6069 6101 6117 6154 6170 6203.5 6258.6 Å
I
6017 (1-5)
6047 (6-10)
6086 (5-8)
6105 Å (0-2)
A
6000
6100
6200
(v''→v') (3-4) (0-0) (5-5) (1-0) (2-0)
6171 6203.5 6228 6259 6315 Å
I
6224 Å (4-4)
B
6200
6300
6400
λ (Å)

Figure III.9. A trace of the fluorescence-monitored $A0_g^+ \rightarrow G0_u^+$ absorption spectrum in the 6200–6500 Å range, showing $v'' \rightarrow v'$ assignments. A: experimental spectrum generated by the probe laser scan; the dashed curve indicates relative dye laser output power. B: computer-generated spectrum showing $v'' \rightarrow v'$ components with peak amplitudes based on the Boltzmann vibrational distribution in the $A0_g^+$ state.

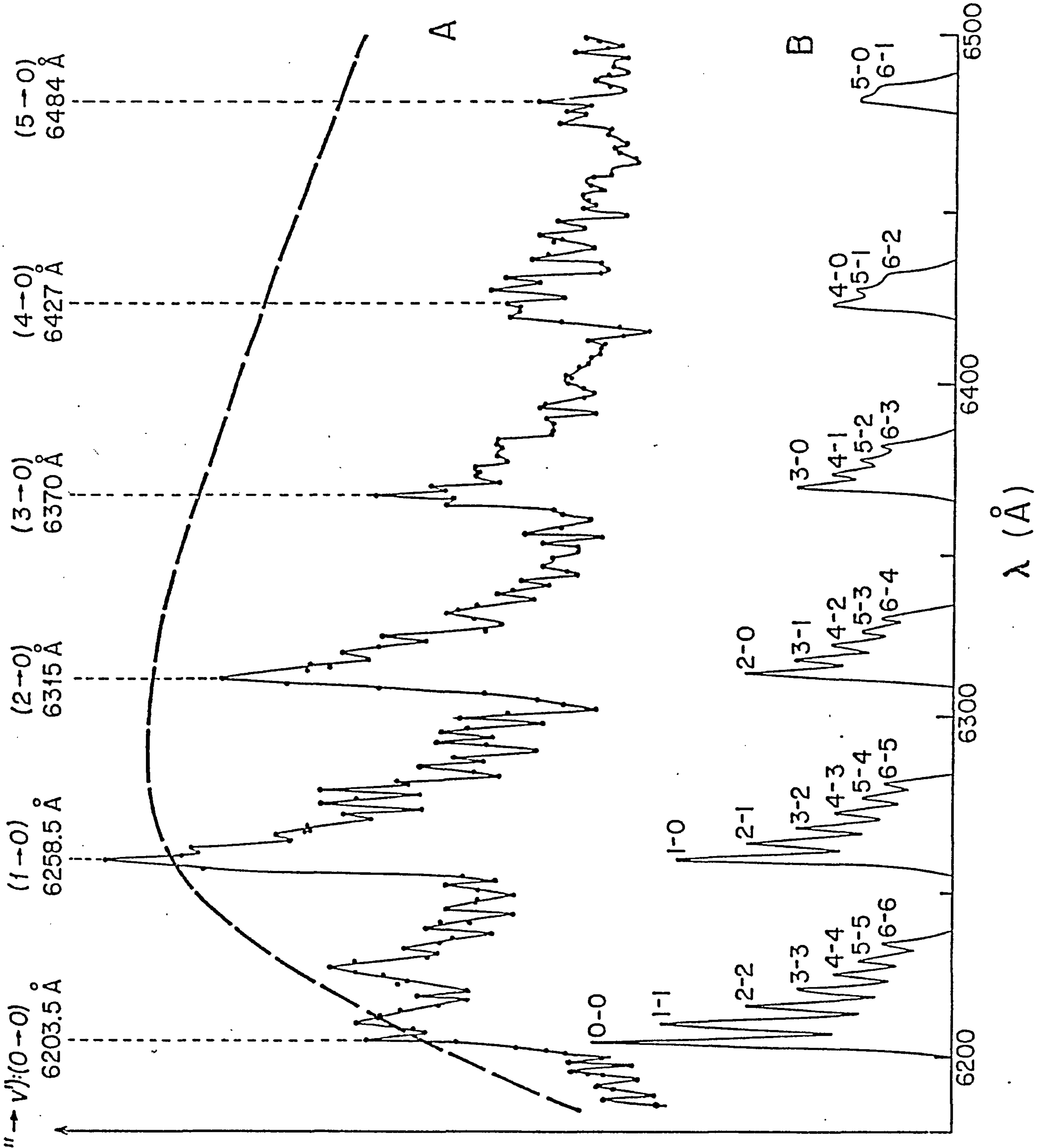
(v''→v'):(0→0)
6203.5 Å
(1→0)
6258.5 Å
(2→0)
6315 Å
(3→0)
6370 Å
(4→0)
6427 Å
(5→0)
6484 Å
I
A
B
0-0
1-1
2-2
3-3
4-4
5-5
6-6
1-0
2-1
3-2
4-3
5-4
6-5
2-0
3-1
4-2
5-3
6-4
3-0
4-1
5-2
6-3
4-0
5-1
6-2
5-0
6-1
6200
6300
6400
6500
λ (Å)

from the traces in Figs. III.7-III.9, each of which covers a relatively narrow spectral range (200-300 Å); consequently, the monotonic variation in signal intensity with wavelength tends to be obscured by variations in the probe laser output power, which are much more pronounced. This behaviour of the fluorescence intensity is most likely due to a difference in the internuclear separations in the $A0_g^+$ and $G0_u^+$ states (Mies et al. 1978). Such a configuration favors transitions from low v" levels of the $A0_g^+$ state to higher v' levels of the $G0_u^+$ state, in accordance with the Franck-Condon principle. The variation of the electronic transition moment, which in this case decreases with increasing internuclear distance (ibid.) may also be partly responsible for the effect.

The band structures shown in Figs. III.7-III.9 lend themselves to interpretation, particularly where the wavelength of the exciting probe radiation is in the region 5975-6500 Å and the spectrum exhibits a fairly high degree of periodicity. The general features of the spectrum in the vicinity of the v"=0⟶v'=0 transition can be interpreted with the aid of Fig. III.5. It is still possible to populate the v'=0 state using radiation of $\lambda > 6203.5$ Å, though then the transitions take place from vibrational states v">0. As the probe radiation is scanned towards longer wavelengths one should expect to observe fluorescence peaks arising from the progression v"⟶v'=1⟶0, 2⟶0, 3⟶0, etc., with a regular v" spacing.

Since the $A0_g^+$ state is metastable, its vibrational levels have a Boltzmann distribution which should cause the fluorescence peaks to fade gradually towards longer wavelengths. This effect is apparent in the spectra shown in Figs. III.8B and 9. The fluorescence peaks constituting the v" progression also contain fluorescence due to other transitions. For instance, the 1⟶0 peak contains contribution from 2⟶1 and 3⟶2 transitions, the 2⟶0 peak from 3⟶1 and 4⟶2 transitions, etc. Because the vibrational spacing in the $G0_u^+$ state is slightly smaller than in the $A0_g^+$ state, the absorption components corresponding to higher v' levels have slightly longer wavelengths than the band-heads and the bands are degraded towards the red. In certain cases, these subsidiary components can be comparable with or even more intense than the band-head because of more favourable Franck-Condon factors. Such seems to be the case with the v"=0⟶v'=0 band-head in Fig. III.8B (λ=6203.5 Å), where some of the other transitions (most likely 4⟶4 and 5⟶5) appear to be exceptionally strong.

As may be seen in Figs. III.7 and 8A, when scanning from λ=6203.5 Å towards shorter wavelengths, the structure of the spectra becomes more complex. A few prominent peaks can still be distinguished, but the spacing between them is irregular, suggesting a dominant role of the Franck-Condon factors as compared with the Boltzmann distribution. Such a hypothesis is quite reasonable if it is considered that the vibrational spacing of the $A0_g^+$ state near the bottom of the well is about 140 cm^{-1} and the temperature of the Hg vapour was maintained at about 700 K, resulting in $kT \simeq 490$ cm^{-1}. The relative vibrational population distribution can be estimated from the Boltzmann factors [exp(-G(v")/kT)] to be 1 : 0.75 : 0.56 : 0.42 : 0.32 for v"=0, 1, 2, 3, 4, respectively. This represents a relatively small variation compared with possible variations in Franck-Condon factors which, even for neighboring transitions, can differ by an order of magnitude (Condon 1947). As a consequence of this situation, the most intense peaks need not correspond to absorption transitions originating from the v"=0 level as might be expected exclusively on the basis of the Boltzmann distribution. Moreover, the value $kT=490$ cm^{-1} represents the lower limit of the actual kinetic temperature of the mercury vapour in the fluorescing region. Stock et al. (1978) showed that the kinetic temperature is usually increased through the absorption of pump laser radiation and approaches the ambient vapour temperature only after a certain relaxation time. Under such circumstances the thermal distribution of vibrational levels would be more uniform, further increasing the relative influence of the F-C factors on the intensity distribution in the spectrum. This argument provides a qualitative explanation for some of the structures in Figs. III.7 and 8A; a quantitative representation of the intensity distribution would be much more difficult and was not attempted.

In order to carry out an analysis of the spectrum, the measured wavelengths of the various peaks were substituted in Eq. (III.4), together with values of ω_e'' and $\omega_e''x_e''$ for the $A0_g^+$ state (Niefer et al. 1983b; Callear and Lai 1980), and the fitting procedure yielded the vibrational constants of the $G0_u^+$ state. It appeared, though, that for peaks far removed from the wavelength of the $v''=0 \longrightarrow v'=0$ transition, the fitting process became sensitive to even small variations (±1 cm^{-1}) in ω_e''. A simple computer program was devised to simulate the spectral profile (without taking into account the unknown F-C factors) and to generate the positions of the peaks corresponding to various transitions in absorption. The best fit was obtained with $\omega_e''=143$ cm^{-1} and $\omega_e''x_e''=0.5$ cm^{-1}, in good agreement with the values reported by Callear and Lai (1980) and by Niefer et al. (1983b). The resulting values of ω_e' and $\omega_e'x_e'$ are listed in Table III.4.

TABLE III.4. Vibrational constants of the $A0_g^+$ and $G0_u^+$ states

Hg_2 state	$\omega_e (cm^{-1})$	$\omega_e x_e (cm^{-1})$
$A0_g^+$	143 ± 2[a]	0.5 ± 0.2[a]
	143[b]	
	144 ± 1[c]	0.5 ± 0.1[c]
$G0_u^+$	129.7 ± 2.0[a]	0.35 ± 0.15[a]

[a] this investigation

[b] Callear and Lai (1980)

[c] Niefer et al. (1983b)

IV. SUMMARY AND CONCLUSIONS

Collisional processes involving excited Rb atoms and Hg_2 'excimers' were investigated by laser-induced fluorescence spectroscopic methods.

In the first part of the investigation, two-photon absorption was used to selectively populate fine-structure sublevels of n^2D Rb states. A photon-counting technique was employed to record the resulting fluorescence spectrum and determine cross sections for fine-structure mixing and quenching in 6^2D, 7^2D and 8^2D states of Rb, due to collisions with ground state Rb atoms, noble-gas atoms and N_2 molecules, which are listed in Tables II.5, II.7-9. The experiment has led to the following conclusions:

(i) the cross sections for fine-structure mixing by collisions with noble gases and N_2 molecules are in the range 5×10^{-14} cm^2 - 26×10^{-14} cm^2 and the quenching cross sections do not exceed about 10% of the mixing cross sections;

(ii) the variation of the noble-gas cross sections with the principal quantum number n of the Rb atom (n=6,7,8) does not follow a general scheme, the trends differ for the various noble gases;

(iii) the variation of the fine-structure mixing cross sections for a given n, from one noble gas to another, correlates with the variation of the free electron - noble gas elastic scattering cross section calculated at the free electron velocity corresponding to the velocity of the particular nD-orbital electron;

(iv) the cross sections for fine-structure mixing in collisions with ground-state Rb atoms are generally larger by a factor 2-5 than the noble gas cross sections, reflecting a longer-range interaction between ground-state and excited Rb atoms. The Rb^*-Rb cross sections are comparable with the geometrical cross sections σ_g of atoms in the appropriate quantum states (Bethe and Salpeter 1955).

In the second part of this investigation, a 'pump and probe' technique was used to excite the $G0_u^+$ state of the Hg_2 excimer (correlated with the 6^1P_1 Hg state). Methods of time-resolved fluorescence spectroscopy were then used to analyze the spectrum resulting from the $G0_u^+ \rightarrow X0_g^+$ decay. The experimental results yielded:

(i) the energy spacing of 16122.0±5.0 cm^{-1} between the potential minima of the $A0_g^+$ and $G0_u^+$ states;

(ii) the wavelength of 2225±2 Å, corresponding to the $v'=0(G0_u^+) \rightarrow X0_g^+$ (bound-free) transition;

(iii) the approximate lifetime of the $G0_u^+$ state, which was found to be of the order of 1 ns.

The vibrational structure of the absorption spectrum, corresponding to the $A0_g^+ \rightarrow G0_u^+$ electronic transition, has been recorded by monitoring the fluorescent decay of the $G0_u^+$ state. An analysis of the spectrum yielded:

ω_e'=129.7±2.0 cm-1, $\omega_e'x_e'$=0.35±0.15 cm-1 for the $G0_u^+$ state and ω_e''=143±2 cm^{-1}, $\omega_e''x_e''$=0.5±0.2 cm^{-1} for the $A0_g^+$ state; the latter two values are in very good agreement with results reported earlier by Callear and Lai (1980) and Niefer et al. (1983b).

An obvious and immediate extension of the Hg_2 experiments would be a study of the fluorescence spectrum (expected to be in the 6900-7000 Å region), resulting from bound-bound transitions between the vibrational levels of the $G0_u^+$ and $B1_g$ states (see Fig. I.1). Such an experiment would yield the vibrational constants of the $B1_g$ state, as well as the energy spacing between the $G0_u^+$ and $B1_g$ states and, indirectly, between the $A0_g^+$ and $B1_g$ states.

REFERENCES

Anderson, E. M. and Zilitis, V. A., 1964. *Opt. Spektrosk.*, 16, 382 [*Opt. Spectrosc. (USSR)*, 16, 211].

Baylis, W. E., 1977. *J. Phys. B: Atom. Molec. Phys.*, 10, L583.

Bennewitz, H. G. and Dohmann, H. D., 1965. *Z. Physik*, 182, 524.

Bethe, H. and Salpeter, E. E., 1955. Handbuch der Physik, Vol. XXXV, edited by Siegfried Flügge (Springer-Verlag, Berlin), p. 88.

Biraben, R., Beroff, K., Grynberg, G. and Giacobino, E., 1979. *J. Physique*, 40, 519.

Callaway, J. and Bauer, E., 1965. *Phys. Rev.*, 140, A1072.

Callear, A. B. and Lai, K. L., 1979. *Chem. Phys. Lett.*, 64, 100.

Callear, A. B. and Lai, K. L., 1980. *Chem. Phys. Lett.*, 75, 234.

Callear, A. B. and Lai, K. L., 1982. *Chem. Phys.*, 69, 1.

Ciuryło, J. and Krause, L., 1982. *JQSRT*, 28, 457.

Condon, E. U., 1928. *Phys. Rev.*, 32, 858.

Condon, E. U., 1947. *Amer. J. Phys.*, 15, 365.

Cooke, W. E. and Gallagher, T. F., 1980. *Phys. Rev. A*, 21, 588.

Coulson, C. A., 1958. Valence (Oxford University Press).

Cuvellier, J., Mestdagh, J. M., Ferray, M. and de Pujo, P., 1983. *J. Chem. Phys.*, 79, 2848.

Dalgarno, A. and Kingston, R. E., 1960. *Proc. Roy. Soc. (London), Ser. A*, 259, 424.

Deech, J. S., Luypaert, R., Pendrill, L. R. and Series, G. W., 1977. *J. Phys. B: Atom. Molec. Phys.*, 10, L137.

Drullinger, R. E., Hessel, M. M., and Smith, E. W., 1977. *J. Chem. Phys.*, 66, 5656.

Ehrlich, D. J. and Osgood, R. M., 1978. *Phys. Rev. Lett.*, 41, 547.

Ehrlich, D. J. and Osgood, R. M., 1979. *Chem. Phys. Lett.*, 61, 150.

Farley, J. W. and Wing, W. H., 1981. *Phys. Rev. A*, 23, 2397.

Fermi, E., 1934. *Nuovo Cimento*, 11, 157.

Franck, J., 1925. *Trans. Faraday Soc.*, 21, 536.

Franck, J. and Grotrian, W., 1921. *Z. Physik*, 4, 89.

Gallagher, A., 1968. *Phys. Rev.*, 172, 88.

Gallagher, T. F., Edelstein, S. A. and Hill, R. M., 1977. *Phys. Rev. A*, 15, 1945.

Głódź, M., Atkinson, J. B. and Krause, L., 1981. *Can. J. Phys.*, 59, 548.

Gounand, F., Fournier, P. R. and Hugon, M., 1979. abstracts of contributed papers, XI International Conference on the Physics of Electronic and Atomic Collisions, Kyoto, edited by K. Takayanaki and N. Oda (The Society for Atomic Collision Research, Japan).

Hahn, Y., 1981. *J. Phys. B: Atom. Molec. Phys.*, 14, 985.

Hamada, H., 1931. *Phil. Mag.*, 12, 50.

Hay, P. J., Dunning, T. H and Raffenetti, R. C., 1976. *J. Chem. Phys.*, 65, 2679.

Herzberg, G., 1950. Spectra of Diatomic Molecules (New York, van Nostrand Publ. Co.).

Hill, R. H., Schuessler, H. A. and Zollars, B. G., 1982. *Phys. Rev. A*, 25, 834.

Hrycyshyn, E. S. and Krause, L., 1970. *Can. J. Phys.*, 48, 2761.

Hugon, M., Gounand, F., Fournier, P. R. and Berlande, J., 1979. *J. Phys. B: Atom. Molec. Phys.*, 12, 2707.

Hugon, M., Gounand, F., Fournier, P. R. and Berlande, J., 1980a. *J. Phys. B: Atom. Molec. Phys.*, 13, 1585.

Hugon, M., Gounand, F. and Fournier, P. R., 1980b. *J. Phys. B: Atom. Molec. Phys.*, 13, L109.

Humphrey, L. M., Gallagher, T. F., Cooke, W. E. and Edelstein, S. A., 1978. *Phys. Rev. A*, 18, 1383.

Jefimenko, O., 1963. *J. Chem. Phys.*, 39, 2457.

Krause, L., 1975. in The Excited State in Chemical Physics, edited by J. W. McGowan (John Wiley, New York).

Littman, M. G., 1978. *Opt. Lett.*, 3, 138.

Loree, T. R., Sze, R. C. and Barker, D. L., 1977. *Appl. Phys. Lett.* 31, 37.

Lundberg, H. and Svanberg, S., 1976. *Phys. Lett.*, 56A, 31.

Marek, J. and Münster, P., 1980. *J. Phys. B: Atom. Molec. Phys.*, 13, 1731.

Masnou-Seeuws, F., Boulmer, J., Maurin, T., Roche, A. L. and Valiron, P., 1982. *J. Phys. B: Atom. Molec. Phys.*, 15, 2989.

Massey, H. S. W. and Burhop, E. H. S., 1952. Electronic and Ionic Impact Phenomena (Oxford, Clarendon Press).

Mies, F. H., Stevens, W. J. and Krauss, M., 1978. *J. Mol. Spectr.*, 72, 303.

Migdałek, J. and Baylis, W. E., 1979. *Can. J. Phys.*, 57, 1708.

Mosburg, E. R and Wilke, M. D., 1977. *J. Chem. Phys.*, 66, 5682.

Mrozowski, S., 1930. *Z. Physik*, 62, 314.

Mrozowski, S., 1934. *Acta Phys. Polon.*, 3, 215.

Mrozowski, S., 1937. *Z. Physik*, 104, 228; 106, 458.

Mrozowski, S., 1944. *Rev. Mod. Phys.*, 16, 160.

Mulliken, R. S., 1971. *J. Chem. Phys.*, 55, 309.

Nesmeyanov, A. N., 1963. Vapour Pressure of the Elements (Academic Press, New York).

Niefer, R. J., 1983. *Ph.D. Thesis*, University of Windsor.

Niefer, R. J., 1985. *Private Communication*.

Niefer, R. J., Atkinson, J. B. and Krause, L., 1983a. *J. Phys. B: Atom. Molec. Phys.*, 16, 3531.

Niefer, R. J., Atkinson, J. B. and Krause, L., 1983b. *J. Phys. B: Atom. Molec. Phys.*, 16, 3767.

Omont, A., 1977. *J. Physique*, 38, 1343.

Pace, P. and Atkinson, J. B., 1974. *Can. J. Phys.*, 52, 1635.

Parker, J. W., Schuessler, H. A., Hill, R. H. and Zollars, B. G., 1984. *Phys. Rev. A*, 29, 617.

Pascale, J., 1978. *J. Chem. Phys.*, 69, 2788.

Phillips, F. S., 1913. *Proc. Roy. Soc. (London)*, A89, 39.

de Prunelé, E. and Pascale, J., 1979. *J. Phys. B: Atom. Molec. Phys.*, 12, 2511.

Rosiński, K. and Sirko, L., 1984. in Abstracts of 16-th European Group for Atomic Spectroscopy Conference, London, edited by A. P. Thorne (European Physical Society, London).

Siara, I. N. and Krause, L., 1973. *Can. J. Phys.*, 51, 257.

Siara, I. N., Dubois, R. U. and Krause, L., 1982. *Can. J. Phys.*, 60, 239.

Smith, E. W., Drullinger, R. E., Hessel, M. M. and Cooper, J., 1977. *J. Chem. Phys.*, 66, 5667.

Stock, M., Smith, E. W., Drullinger, R. E. and Hessel, M. M., 1977. *J. Chem. Phys.*, 67, 2463.

Stock, M., Smith, E. W., Drullinger, R. E. and Hessel, M. M., 1978. *J. Chem. Phys.*, 68, 4167.

Supronowicz, J., Atkinson, J. B. and Krause, L., 1984. *Phys. Rev. A*, 30, 112.

Supronowicz, J., Atkinson, J. B. and Krause, L., 1985. *Phys. Rev. A*, 31, 2691.

Takeyama, H., 1952. *J. Sci. Hiroshima Univ.*, A15, 235.

Tam, A. C., Yabuzaki, T., Curry, S. M., Hou, M. and Happer, W., 1978. *Phys. Rev. A*, 17, 1862.

Tellinghuisen, J., 1975. *Phys. Rev. Lett.*, 34, 1137.

Theodosiou, C. E., 1984. *Phys. Rev. A*, 30, 2881.

Wolnikowski, J., Atkinson, J. B., Supronowicz, J. and Krause, L., 1982. *Phys. Rev. A*, 25, 2622.

Woodgate, G. K., 1970. Elementary Atomic Structure (McGraw-Hill, London).

Zollars, B. G., Schuessler, H. A., Parker, J. W. and Hill, R. H., 1983. *Phys. Rev. A*, 28, 1329.

VITA AUCTORIS

I was born on August 17, 1955 in Warsaw, Poland. After graduation from secondary school in 1974, I entered the Physics Department at the University of Warsaw, where in 1979 I obtained my Master's Degree in atomic spectroscopy. During years 1979-1981 I was on the staff of the Institute of Geophysics of the Polish Academy of Sciences in Warsaw. I arrived in Canada in 1981 and enrolled in the Ph.D. program in Physics at the University of Windsor. During part of my graduate studies I received financial assistance from the University of Windsor in the form of a graduate scholarship.